J. Fluid Mech. (2025), *vol.* 1009, A7, doi:10.1017/jfm.2025.180

Harmonic decomposition of forces and estimates of reduced mean flow in jackets subjected to waves and current

Aidan J. Archer[1], **Paul H. Taylor**[1], **Hugh Wolgamot**[1,2], **Jana Orszaghova**[1,2] **and Saishuai Dai**[3]

[1]School of Earth and Oceans, University of Western Australia, Perth, WA 6009, Australia

[2]Marine Energy Research Australia, Great Southern Marine Research Facility, Albany, WA 6330, Australia

[3]Naval Architecture, Ocean and Marine Engineering Department, University of Strathclyde, Glasgow, UK

Corresponding author: Aidan J. Archer, aidan.archer@research.uwa.edu.au

(Received 23 July 2024; revised 3 February 2025; accepted 7 February 2025)

The interaction between porous structures and flows with mean and oscillatory components has many applications in fluid dynamics. One such application is the hydrodynamic forces on offshore jacket structures from waves and current, which have been shown to give a significant blockage effect, leading to a reduction in drag forces. To better understand this, we derived analytical expressions that describe the effect of current on drag forces from large waves, and conducted experiments that measured forces on a model jacket in collinear waves and currents. We utilised symmetry and phase-inversion techniques, relying on the underlying physics of wave structure interaction, to separate Morison drag and inertia-type forces and to decompose these forces into their respective frequency harmonics. We find that the odd harmonics of the drag force mostly contain the loads from waves, while even harmonics vary much more rapidly with the current speed flowing through the jacket. At the time of peak force, these current speeds were estimated to be 40 % of the undisturbed current and 50 % of the industry-standard estimates, a result that has significant implications for design and re-assessment of jackets. At times away from the peak force, when there are no waves and only current, the blockage effects are reduced. Hence, the variation in blocked current speeds appears to occur on a relatively fast time scale similar to the compact wave envelope. These findings may be generalisable to any jacket-type structure in flows with mean and high Keulegan–Carpenter number oscillatory components.

Key words: surface gravity waves, wave–structure interactions

© The Author(s), 2025. Published by Cambridge University Press. This is an Open Access article, distributed under the terms of the Creative Commons Attribution licence (https://creativecommons.org/licenses/by/4.0/), which permits unrestricted re-use, distribution and reproduction, provided the original article is properly cited.

https://doi.org/10.1017/jfm.2025.180 Published online by Cambridge University Press

1. Introduction

Jackets are commonly used as support structures for offshore oil and gas platforms and, more recently, for offshore wind turbines and sub-stations. They are fixed, bottom-founded steel structures, comprising numerous slender cylindrical members and assembled as a spaceframe. Efficient jacket design is contingent on accurate estimates of the hydrodynamic forces from waves and currents. However, the impact of combined waves and current on these hydrodynamic forces is not fully understood even now. In current design standards (ISO 2020; API 2000), wave and current forces are treated with a Morison-type approximation (Morison *et al.* 1950) of the general form

$$F = \underbrace{(\cdots)\frac{\partial u_w(t)}{\partial t}}_{\text{Inertia}} + \underbrace{(\cdots)\,(u_w(t)+u_{cs})\,|u_w(t)+u_{cs}|}_{\text{Drag}}\,. \tag{1.1}$$

This approximation assumes the fluid loading comprises an inertia term that results from the acceleration of the irrotational flow around a structure, and a drag term that results from shed vorticity (Lighthill 1986). The wave-induced horizontal fluid velocity that varies in time t is denoted u_w, and u_{cs} is the mean fluid velocity through the jacket from a steady current (referred to in this paper as the blocked current). The form of (1.1) is only indicative of the full expression to highlight the role of waves and current on force. The inertia and drag coefficients (implicit in the $(\cdots)$ terms) are assumed independent of the amplitude and period of $u_w(t)$ (i.e. no Keulegan–Carpenter (KC) number effects), which is appropriate for large KC number regimes like large waves on jacket structures. The complete inertia term also contains convective derivative terms (e.g. the higher-order Faltinsen, Newman & Vinje (FNV) model; see Kristiansen & Faltinsen (2017)), which are ignored here but are revisited in § 5.2.1. In present design standards, u_w is approximated by its value if the structure was not present, while u_{cs} is reduced from the undisturbed current speed u_c by accounting for simple current blockage, a flow effect where the presence of the jacket acts as an obstacle array, reducing local fluid velocities and accompanying drag forces in the absence of waves (Taylor 1991). For design wave loads on jackets, drag forces generally dominate over inertia forces as the width of structural members are small compared with the incident wavelength and are of the order of the wave amplitude or smaller. These drag-dominated conditions hold in general for porous structures subjected to high Keulegan–Carpenter number oscillatory flows. Actuator disc models, which represent the bulk flow interaction with porous structures, actually disregard the inertia forces as they give zero mean force over an oscillation period and are therefore assumed to have no effect on the flow field (see e.g. Taylor *et al.* 2013; Archer *et al.* 2024*a*).

Although jackets may not be what one usually imagines when they think of porous structures, they have been described this way since Taylor (1991) first proposed current blockage. Similarly, propellers and turbines have been characterised this way for much longer (e.g. Taylor 1944). While we frame our discussion with regard to offshore jacket structures, our methods may be applicable to other porous structures in similar flow regimes, with recent work (e.g. Cicolin *et al.* 2024; Seol *et al.* 2024) confirming the ongoing interest in drag loads on porous structures in multiple contexts.

The Morison-based force estimation (1.1) does not account for the additional effects that arise from the combined action of waves and currents, namely a flow effect called 'wave-current blockage' where the blocked current u_{cs} is further reduced from combined waves and current compared with the reduction from current alone. This effect confounded early attempts to simply interpret the results of jacket tests in combined wave and current (e.g. Allender & Petrauskas 1987), until the theory was updated by Taylor *et al.* (2013).

https://doi.org/10.1017/jfm.2025.180 Published online by Cambridge University Press

Wave-current blockage is driven by the additional mean drag force acting over a wave period, which has been studied in previous experiments that tested in-line currents combined with regular waves (Santo *et al.* 2014; Archer *et al.* 2024*b*) and combined with focused wave groups (Santo *et al.* 2018*a*,*b*). Most of these studies tested scale models of structurally dense offshore oil and gas jackets, which elicit stronger blockage effects than the lightweight, structurally sparse jackets supporting individual wind turbines, but Archer *et al.* (2024*b*) showed that these effects are still significant for lightweight jackets. Moreover, most offshore wind farms have an additional jacket supporting an offshore electrical substation; these jackets are dense (like oil and gas jackets), with very high deck loads to be supported and many J-tubes housing electrical cables. Therefore, improving jacket design standards to account for wave-current blockage is important as it will lead to a reduction in estimated drag loads and hence a reduction in costs of offshore wind farms. However, modelling wave-current blockage presently requires computational fluid dynamic solvers that are time consuming to set up and run and difficult to validate (and still rely on additional assumptions as the flow around individual structural members cannot be fully resolved in the flow regimes relevant at full scale).

In this paper, we analyse the forces from combined waves and current and assess them for evidence of wave-current blockage. These forces act at a range of frequencies, including higher harmonics (above the linear wave frequency range) that can coincide with the natural frequency of a real jacket (typically designed to be $> 2-3$ times the incident wave frequency). We hypothesise that the blocked current u_{cs} is significantly reduced during the loading from large waves, and that the effects of this blocked current are mostly contained in even drag force harmonics. Comparatively, odd harmonics mainly contain drag forces from only waves. The theory supporting this hypothesis is outlined in § 2. To assess this, we analysed experimental force measurements of two model jackets in combined waves and currents. Our broader aim is to investigate if wave-current blockage effects can be accurately estimated without needing computational fluid dynamic solvers; the work in this paper is a step towards this aim.

The paper follows the following structure. In § 2 we derive expressions which indicate the contribution of current to different drag force harmonics. We then present the experimental set-up in § 3, an overview of the quality of the measurements in § 4 and further analysis in § 5. Within this analysis, we attempt to separate drag and inertia force contributions in § 5.2, we estimate the reduction in local current speeds due to wave-current blockage effects in § 5.3 and we use these estimates to recreate the total force time histories in § 5.4. We draw conclusions in § 6.

2. Contribution of current to drag force harmonics in large waves

The Morison drag term in (1.1) contains force components from purely waves ($u_w \times u_w$), from waves and current ($u_w \times u_{cs}$) and from purely current ($u_{cs} \times u_{cs}$), but the contribution from each of these components to force harmonics at different frequencies is not clear. To demonstrate this complexity, we define the nonlinear wave-driven horizontal fluid velocity u_w, which can be written to third order in wave steepness (Stokes 1847) as

$$u_w = u_{11} + u_{20} + u_{22} + u_{31} + u_{33} + \dots . \tag{2.1}$$

The terms on the right-hand side of the expression follow the structure u_{ij}, where the subscript i denotes the order of each term given by the power of the linear wave amplitude, and the subscript j denotes the harmonic in frequency given by the multiplier of the linear ($j = 1$) frequency. The expansion of terms follow the general property of a Stokes expansion, that for a given i, $j = i,\ i-2,\ i-4,\ \dots$ so long as $j \geq 0$. In the

https://doi.org/10.1017/jfm.2025.180 Published online by Cambridge University Press

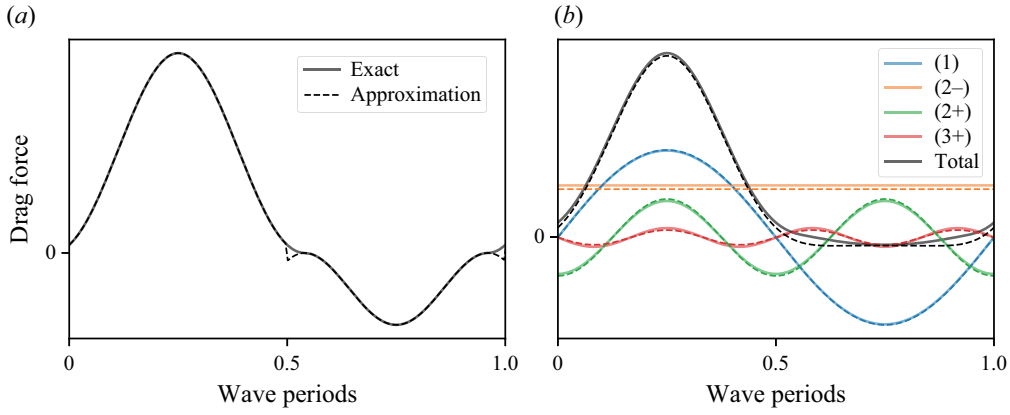

Figure 1. Comparison of exact forms of Morison drag (solid lines) with the approximations derived in this paper (dashed lines), for a regular wave case where $u_w/u_{cs} = 4$. In (*a*), the full form in (1.1) is compared with the approximation (2.2). In (*b*), the drag force harmonic approximations in table 2 (which account for variations in wave kinematics with depth and variations of the free surface) are compared with numerically evaluated solutions for the force on a vertical member spanning the full depth of the water column and protruding above the free surface.

Morison equation, this Stokes structure (i.e. the relationship between the order i and the harmonic j) is maintained for the inertia term but no longer holds for the drag term because the function $u|u|$ is non-analytic. Perfect separation of wave and current drag force components in frequency is therefore not possible, but an approximate separation may be. We explore this possibility here.

To attempt to separate wave and current drag force components in frequency, we consider the flow regime where wave kinematics are much larger than the blocked current ($u_w \gg u_{cs}$), which is true for large design waves for offshore structures in the region close to the free surface where the wave kinematics are largest. In this regime, we can approximate the Morison drag expression in (1.1) as

$$\text{Drag} \approx (\cdots)\left(u_w(t)|u_w(t)| + 2|u_w(t)|u_{cs} + \text{sgn}(u_w)u_{cs}^2\right), \tag{2.2}$$

where $\text{sgn}(u_w)$ is a sign function, equal to 1 when $u_w > 0$ and -1 when $u_w < 0$. The approximation was first given in Haritos (2007) (but without the $\text{sgn}(u_w)u_{cs}^2$ term) to model the interaction between waves and structural motion. It was used by Santo *et al.* (2018*a*) to estimate the drag forces on a dynamically responding jacket, showing good agreement with experimental data and with more complex numerical models. The approximation can be (partially) explained by expanding the full Morison drag form in (1.1) at wave crests and troughs. Combining the expanded expressions at wave crests, $u_w^2 + 2u_w u_{cs} + u_{cs}^2$, and at troughs, $-u_w^2 - 2u_w u_{cs} - u_{cs}^2$, gives (2.2). However, this does not explain why the approximation performs so well as u_w varies across a wave period, with only very localised poor agreement near zero force – see figure 1(*a*), which compares the approximation with the full form in (1.1) for a regular wave case with $u_w/u_{cs} = 4$ (similar to the regimes we test experimentally). Hence, (2.2) is more of an empirical observation. As the aim of this analysis is to approximate forces from large waves, the very localised poor agreement near zero force is of secondary importance. We are primarily concerned with peak forces, for which the approximation works well.

The approximation (2.2) separates wave × wave, wave × current and current × current drag force terms. To analyse each of these terms, we assume u_w is driven by a regular wave in water depth h

https://doi.org/10.1017/jfm.2025.180 Published online by Cambridge University Press

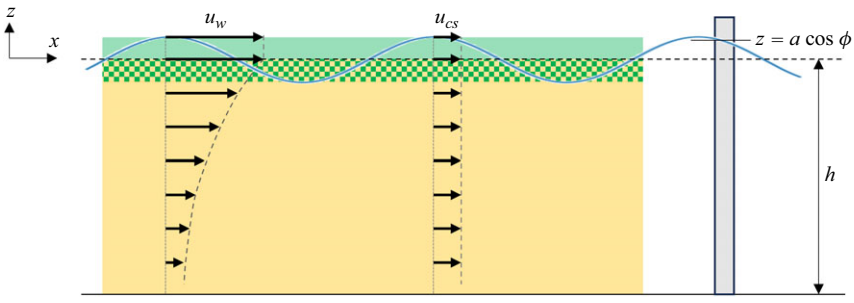

Figure 2. Assumed variation of horizontal kinematics of wave u_w and blocked current u_{cs} with depth. The jacket is represented as a stick, slender compared with the wavelength, as assumed by Tromans *et al.* (1992). The free surface at the jacket is taken as a point estimate of $z = a\cos(\phi)$. Note that u_{cs} actually acts within the jacket, but here we separate it for clarity. To approximate the total Morison drag force acting on the jacket, we split the vertical domain into two regions, a free surface region (■) from $z = 0$ to $z = a\cos(\phi)$, and a mean depth region (■) from $z = 0$ to $z = -h$.

$$u_w(t) \approx \omega a \frac{\cosh(k(z+h))}{\sinh(kh)} \cos(\phi), \tag{2.3}$$

where ω is the angular frequency, a is the wave amplitude, k is the wavenumber, z is the vertical coordinate axis, defined as positive upward with $z = 0$ the mean free surface, and ϕ is the phase angle ($\phi = kx - \omega t$). Here, we make the simplification of omitting all second- and higher-order contributions to u_w (i.e. we only consider the linear contribution, u_{11} in (2.1)). This simplification should be reasonably accurate for cases of interest, as in deep water the second-order super-harmonic contribution to the velocity potential is absent for regular waves and is small for wave groups. Moreover, in Appendix B, we show that the relative force amplification from the addition of a current is well predicted using linear kinematics. See figure 2 for a representation of the variation in u_w and u_{cs} with depth, with u_{cs} assumed to be constant. In reality, u_{cs} varies with depth, partially because currents are often stratified in the ocean, and partially because u_{cs} will increase (i.e. become less blocked) with depth as u_w decays. Because of this, u_{cs} can be thought of as an 'effective' blocked current and is more representative of the current speeds near the free surface which contribute to the majority of the drag loading. Using (2.3), we define two vertical integrals, one over the mean water depth from the seabed at $z = -h$ to the mean free surface at $z = 0$, and one over the varying free surface from $z = 0$ to $z = a\cos(\phi)$. Starting with the wave × wave drag force term, the mean depth integral from $z = -h$ to $z = 0$ gives

$$\int_{-h}^{0} u_w(t)|u_w(t)|\, dz = \frac{\omega^2 a^2}{2k} D \cos(\phi)|\cos(\phi)|, \tag{2.4}$$

where $D = (kh + (1/2)\sinh(2kh))/\sinh^2(kh) \approx 1$ for deep water. The phase component, $\cos(\phi)|\cos(\phi)|$, can be approximated by the Fourier series

$$\cos(\phi)|\cos(\phi)| = \frac{8}{3\pi}\left[\cos(\phi) + \frac{1}{5}\cos(3\phi) + \frac{1}{35}\cos(5\phi) + \ldots\right], \tag{2.5}$$

which consists of an infinite summation of only odd harmonics (see e.g. Orszaghova *et al.* (2021) for the fully expanded form). Note that these integral limits assume the jacket extends to the sea bed, which is always true practically but is not the case for our experimental set-up, see § 3. In Appendix A, we repeat the analysis with adjusted integral bounds to account for this.

https://doi.org/10.1017/jfm.2025.180 Published online by Cambridge University Press

Wave × current, $2\lvert u_w(t)\rvert u_{cs}$		
Mean depth integral	$2\dfrac{\omega a}{k}\lvert\cos(\phi)\rvert u_{cs}$	(2.8)
phase	$\lvert\cos(\phi)\rvert = \dfrac{2}{\pi}\left[1+\dfrac{2}{3}\cos(2\phi)-\dfrac{2}{15}\cos(4\phi)+\dots\right]$	(2.9)
Free surface integral	$2\omega a\lvert\cos(\phi)\rvert u_{cs}\times a\cos(\phi)$	(2.10)
phase	(2.5)	
Current × current, $\mathrm{sgn}(u_w)u_{cs}^2$		
Mean depth integral	$\mathrm{sgn}(u_w)u_{cs}^2\times h$	(2.11)
phase	$\mathrm{sgn}(u_w)\approx\dfrac{4}{\pi}\left[\cos(\phi)-\dfrac{1}{3}\cos(3\phi)+\dfrac{1}{5}\cos(5\phi)+\dots\right]$	(2.12)
Free surface integral	$\mathrm{sgn}(u_w)u_{cs}^2\times a\cos(\phi)=a\lvert\cos(\phi)\rvert u_{cs}^2$	(2.13)
phase	(2.9)	

Table 1. Expressions for the mean depth and free surface integrals, with Fourier series of the associated phase components, for the wave × current and current × current terms in (2.2). See figure 2 to visualise the bounds of these integrals.

The free surface integral from $z=0$ to $z=a\cos(\phi)$ can be approximated as

$$\int_0^{a\cos(\phi)} u_w(t)\lvert u_w(t)\rvert\,dz \approx (\omega a)^2\cos(\phi)\lvert\cos(\phi)\rvert\times a\cos(\phi). \tag{2.6}$$

The phase component in (2.6) can be approximated by the Fourier series,

$$\cos^2(\phi)\lvert\cos(\phi)\rvert = \frac{4}{3\pi}\left[1+\frac{6}{5}\cos(2\phi)+\frac{6}{35}\cos(4\phi)+\dots\right], \tag{2.7}$$

which consists of only even harmonics.

The same analysis is repeated for the wave × current and for the current × current drag force terms in (2.2), integrating each term up the vertical water column, $\int_{-h}^{0}(\cdots)\,\mathrm{d}z$, and up to the varying vertical free surface height, $\int_0^{a\cos(\phi)}(\cdots)\,\mathrm{d}z$. The resulting expressions are summarised in table 1, including expressions (2.8)–(2.13).

The wave × wave, wave × current and current × current drag force terms ((2.4), (2.6), (2.8), (2.10), (2.11) and (2.13)) can be summed and grouped into those acting at each frequency harmonic using the Fourier series defined in (2.5), (2.7), (2.9) and (2.12). The resulting expressions for the first three frequency harmonics, including the second harmonic difference term which contains force components close to zero frequency, are given in table 2. These expressions agree well with numerical evaluations of the exact form – see figure 1(*b*). For brevity, we will refer to the linear harmonic as (1), the second harmonic difference as (2−), the second harmonic sum as (2+) and the third harmonic sum as (3+).

To show the effect of current, each drag force harmonic expression in table 2 is written in the form: a pure wave force term × [a current multiplier]. Within this current multiplier, the blocked current u_{cs} is non-dimensionalised by the phase speed $c=\omega/k$.

https://doi.org/10.1017/jfm.2025.180 Published online by Cambridge University Press

Odd frequency harmonics		
First harmonic (1)	$\frac{4}{3\pi}\frac{\omega^2 a^2}{k}D\left[1+\frac{1}{D}\left(4\frac{u_{cs}}{c}+3\frac{kh}{(ka)^2}\left(\frac{u_{cs}}{c}\right)^2\right)\right]\cos(\phi)$	(2.14)
Third harmonic sum (3+)	$\frac{4}{15\pi}\frac{\omega^2 a^2}{k}D\left[1+\frac{1}{D}\left(4\frac{u_{cs}}{c}-5\frac{kh}{(ka)^2}\left(\frac{u_{cs}}{c}\right)^2\right)\right]\cos(3\phi)$	(2.15)
Even frequency harmonics		
Second harmonic difference (2−)	$\frac{4}{3\pi}\omega^2 a^3\left[1+3\,(ka)^{-2}\frac{u_{cs}}{c}\right]$	(2.16)
Second harmonic sum (2+)	$\frac{8}{5\pi}\omega^2 a^3\left[1+5/3\,(ka)^{-2}\frac{u_{cs}}{c}\right]\cos(2\phi)$	(2.17)

Table 2. Drag force frequency harmonic expressions.

The magnitudes of the u_{cs}^2 terms in the first and third harmonics are small and are only non-negligible for very fast currents. Even harmonic drag forces also have contributions from u_{cs}^2, but these contributions are negligible and hence are omitted from (2.16) and (2.17). As the u_{cs}^2 terms are small in (2.14) and (2.15), the size of each odd harmonic predominantly scales linearly with current, but this scaling is small as the u_{cs} terms are small compared with the pure wave force (as $c \gg u_{cs}$). In contrast, even harmonics have much larger linear modifications from current due to their dependence on the inverse of wave steepness (ka) squared (and $ka < 1$), indicating that wave-current blockage effects are primarily contained in the (2−) and (2+) harmonics.

Not only do the drag force expressions in (2.14)–(2.17) indicate the relative importance of current for each harmonic, they actually enable estimates of the blocked current u_{cs}, given accurate force measurements. These estimates do not require knowledge of the drag coefficient of the structure, just an assumption of the basic structure of wave kinematics, the Morison form of the drag force and the approximate decomposition of Morison drag (2.2). In Appendix A, we show that the numerical scaling factors of the current contribution to odd and even harmonics are slightly affected by the finite height of the jacket model in the experiments, but the basic structure of the solutions does not change. In Appendix B, we validate the accuracy of these expressions in estimating u_{cs} by comparing with Stokes' fifth-order wave theory (Fenton 1990). Although the assumption of linear kinematics in the decomposition is relatively inexact, the relative amplification from the addition of a current is well predicted. Therefore, we expect that the basic structure of these results should hold in real waves, and hence, estimates of the blocked current, accurate enough for engineering analyses, can be obtained. To obtain such estimates of the blocked current, results from physical experiments were analysed. The set-up of these experiments is described next.

3. Experimental set-up and methods

Physical experiments were carried out in the Kelvin Hydrodynamic Laboratory towing tank at the University of Strathclyde, Glasgow. The tank is 76 m long, 4.6 m wide and has a 1.8 m operating water depth. At one end of the tank are four Edinburgh Designs Ltd. hinged flap wavemakers with force feedback control, and at the other end is a sloping beach that acts as a passive absorber. A self-propelled carriage runs along the length of the tank in both directions.

https://doi.org/10.1017/jfm.2025.180 Published online by Cambridge University Press

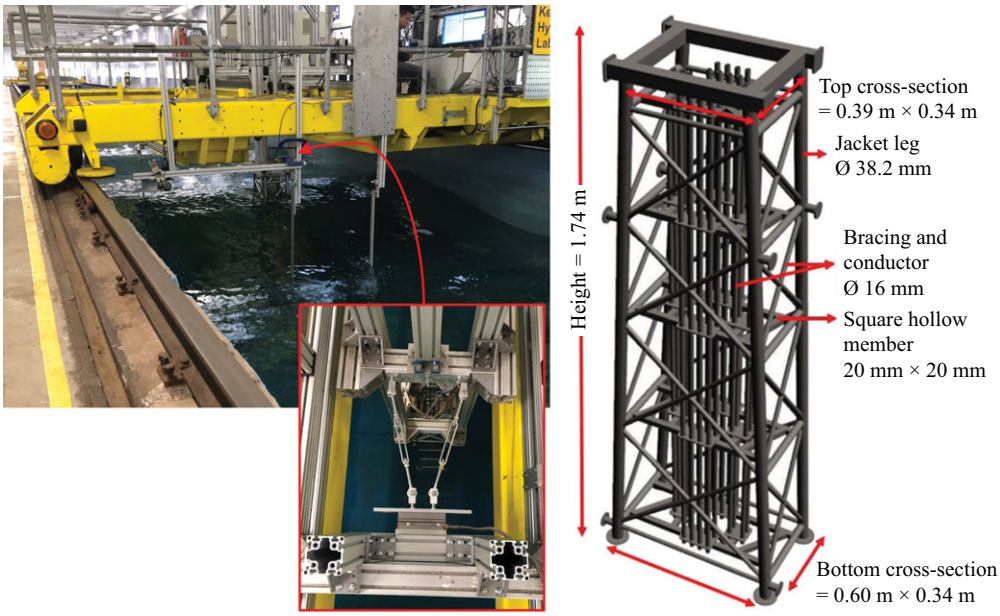

Figure 3. Left photograph shows the carriage with the jacket model suspended underneath, viewed in a down-wave direction. Photo inset is a close-up view of the interface between the jacket mounting frame and the force transducer. Right image shows a three-dimensional computer-aided design (CAD) model of the jacket.

We tested the same jacket model used previously in Santo *et al.* (2018*b*), a 1:80 scale model of a second generation North Sea platform. The density of structural members in the model is also representative of an offshore wind electrical substation jacket. Figure 3 shows the jacket and its relevant dimensions. It stands at 1.74 m tall and is rectangular when viewed end on but tapered when viewed broadside. Cylinders of 38.2 mm diameter make up the four jacket legs, 16 mm diameter cylinders are used for the 24 vertical conductors and for diagonal bracing and 20 mm square tubing forms horizontal support frames. The jacket was oriented end on with its front rectangular face normal to the direction of current and wave propagation.

The jacket was suspended below the carriage from a stiff mounting frame via a double pendulum arrangement, allowing the total in-line horizontal force to be measured by a 6 degree of freedom piezoelectric-type force transducer – see figure 3. The free surface was measured by resistance-based wave probes, both at the jacket by a probe mounted on the carriage between the jacket and the tank wall, and at three fixed locations along the tank, including at the longitudinal tank centre – see figure 7(a) for these fixed positions. All measurements were sampled at 137 Hz and then interpolated to 100 Hz. The distance from the base of the jacket to the still water level was 1.33 m, leaving 0.41 m of the jacket remaining above the water to ensure that the largest wave crests did not hit the mounting frame, and leaving a 0.47 m gap between the base of the jacket and the tank floor to allow the jacket to be towed.

The jacket was towed at constant speed u_c of -0.28, -0.14, -0.07, 0, 0.07, 0.14 and $0.28\ \mathrm{m\ s^{-1}}$ in otherwise still water, representing currents with a uniform depth profile. The fastest $\pm 0.28\ \mathrm{m\ s^{-1}}$ speeds correspond to extreme $2.5\ \mathrm{m\ s^{-1}}$ currents at field scale. We define positive current speeds as acting in the same direction as wave propagation, realised by towing the jacket towards the wavemaker. Positive currents add to the positive wave kinematics in a crest, and negative currents add to the negative kinematics in a wave trough.

https://doi.org/10.1017/jfm.2025.180 Published online by Cambridge University Press

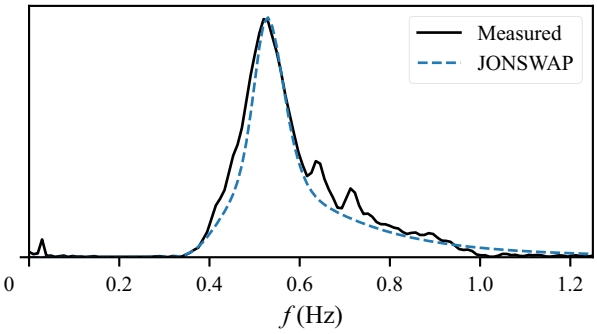

Figure 4. Shapes of the input JONSWAP power spectrum compared with the measured linear free surface amplitude spectrum with no current (linearised using the two-phase combination method (5.1)). The shapes of these should theoretically match, as a focused wave group (or NewWave) is the auto-correlation function in shape at focus (Tromans *et al.* 1991). The good shape match therefore indicates that the intended JONSWAP power spectrum was realised in experiments.

All current speeds were run in combination with NewWave-type focused wave groups which are based on the average shape of a large crest in a random sea (Tromans *et al.* 1991; Walker *et al.* 2004). The focused wave groups had 0.257 m crest amplitudes at focus, and were generated according to a Joint North Sea Wave Project (JONSWAP) power spectrum truncated at 1 Hz with a peak frequency of 0.52 Hz and a gamma of 3.3. Figure 4 shows that the intended shape of the JONSWAP power spectrum was realised in experiments. Both crest-focused (0° phase) and trough-focused (180° phase shifted) wave groups were generated – see figure 5(*a*,*b*) for the shape of the wave groups at focus. The trough-focused wave groups were achieved by simply adding 180° to the phase of each Fourier component of the paddle signal, replacing a crest-focused wave group by a trough-focused one. All wave groups were programmed to focus at the longitudinal tank centre where the fixed wave gauge was positioned. The starting position of the carriage was set for each towing speed such that the jacket always reached the centre of the tank at the time of focus.

In the experiments, a mean linear crest amplitude at focus of 0.213 m was realised, which represents an extreme wave of 17 m linear amplitude and 16 s peak period in 106.4 m water depth, Froude-scaled down to 1:80 laboratory scale. For context, the maximum significant wave height for a 100 year return period in the North Sea is 13.8 m, and the most probable maximum individual wave height scales by 1.17 for every factor of 10 increase in return period (i.e. going from 100 to 1000 years), according to the data in table 1 of Santo *et al.* (2016). The experimental tests therefore represent a 1 in ~ 2000 year extreme wave condition. This is a sensible risk level to test, more severe than the 1 in 10,000 year design condition for unmanned low-consequence structures, but not quite severe enough for some permanently manned structures that are designed to withstand 1 in 10,000 year wave loads. This extreme wave test regime is characterised by high Keulegan–Carpenter numbers, $\mathrm{KC} = 2\pi a/d \approx 35-80$ near the mean free surface (here, d is the diameter of a jacket member). Because KC numbers are high, we expect that the drag behaviour is similar to that for steady flow (or, in other words, we do not expect there to be significant KC effects that are associated with small KC numbers). Physically, the wave-induced oscillations are very large compared with the jacket members' diameter, so when the shed vortices from a wave crest are swept back through the jacket in the subsequent wave trough, any coherent structures in the wake would have mixed out. This wake mixing would be further enhanced by the complex interactions between the vortices shed off each of the many jacket members. This wake mixing behaviour implies that (*a*) the model jacket maintains the same drag coefficient at different current speeds, (*b*) the specific

https://doi.org/10.1017/jfm.2025.180 Published online by Cambridge University Press

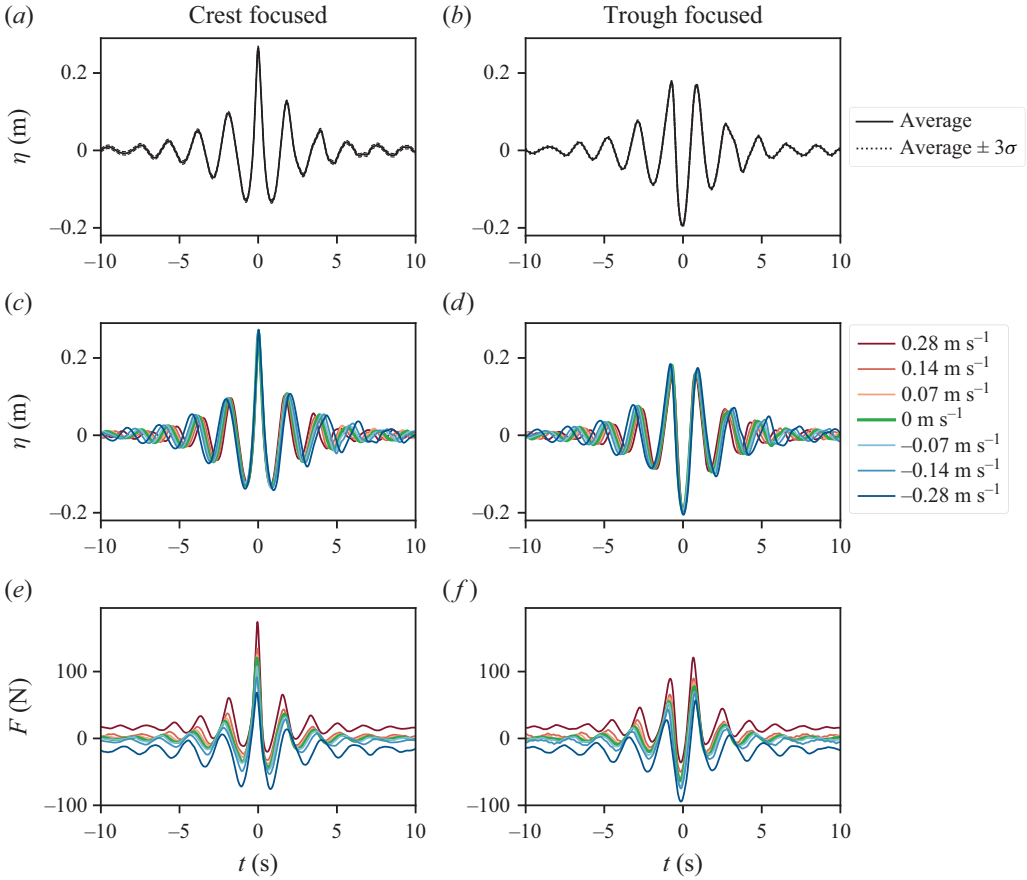

Figure 5. Time series measurements of crest-focused wave groups (left panels) and trough-focused wave groups (right panels). (*a,b*) Free surface recorded by the fixed wave gauge at the longitudinal tank centre, averaged over all tests. (*c,d*) Free surface recorded by the carriage-mounted wave gauge at different current speeds, averaged over repeat tests. *(e,f)* Total force recorded at different current speeds, averaged over repeat tests. All time series are lowpass filtered at 3 Hz.

arrangement of structural members is unimportant (and does not vary much in jackets anyway) and (*c*) the same qualitative observations should hold for all high-KC number extreme wave conditions with combined in-line current.

4. Free surface and total force results

The experimental measurements were highly repeatable, as demonstrated by measurements of the free surface by the fixed wave gauge at the longitudinal tank centre in figure 5(*a,b*). Free surface and force measurements for repeat tests at each current speed have very little deviation from the mean with respective root-mean-square errors below 0.002 m and 1.3 N ($< 2\,\%$ of the peak).

Towing the carriage along the tank to represent a current changes the wave encounter frequency due to the Doppler effect – see the dilation of the time axis for different current speeds in figure 5(*c–f*). Different tow speeds will also cause small differences in the spatial location of the jacket, and hence in the encountered wave form, either side of the focused peak ($t = 0$). However, we expect that this effect is negligible near the focused peak, which

https://doi.org/10.1017/jfm.2025.180 Published online by Cambridge University Press

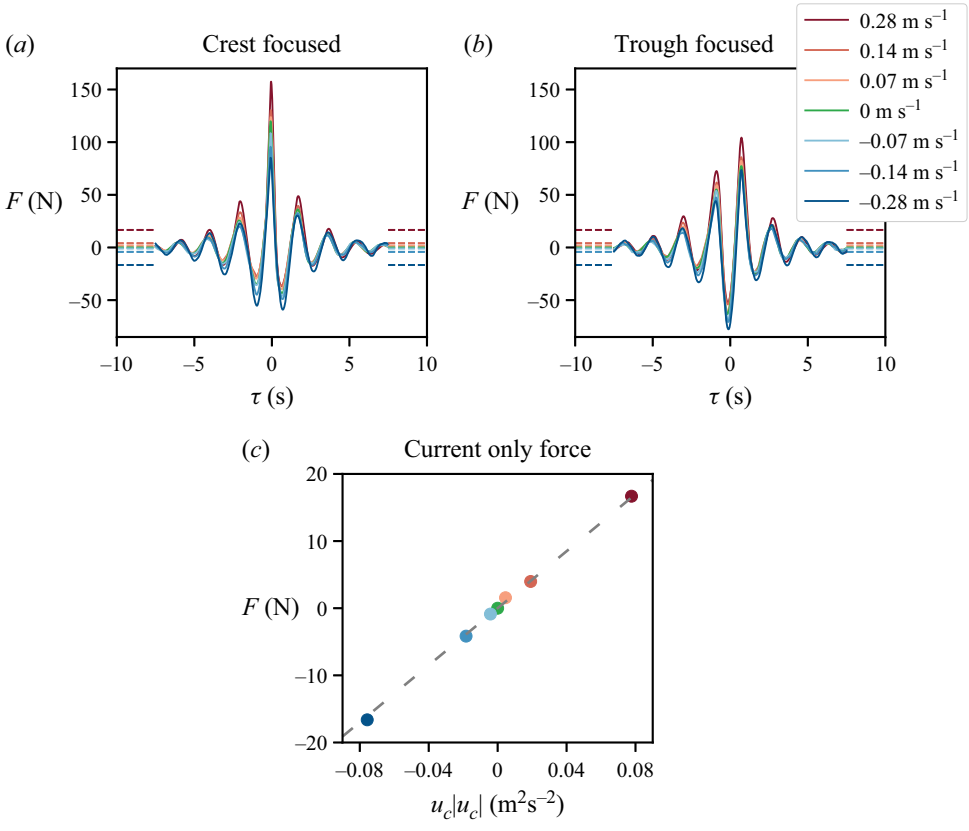

Figure 6. (*a,b*): Total force measurements of crest-focused (*a*) and trough-focused (*b*) wave groups, lowpass filtered at 3 Hz. The time axis has been scaled to account for the Doppler effect, and the mean drag force from current (which is represented as dashed horizontal lines on either side of the focused wave group) has been removed. These current-only forces are plotted again in (*c*), and are shown to scale linearly with $u_c|u_c|$.

is our primary concern. Hence, we assume that wave kinematics are not influenced by towing the carriage. For clarity of comparison, the time axis of subsequent figures (e.g. figure 6) will be scaled to partially account for the Doppler effect. This scaled time is $\tau = t(1 + u_c/c)$, where c is the phase speed of the spectral peak wave frequency observed in a stationary reference frame, and u_c is the carriage speed (i.e. the undisturbed current). While this time scaling does not fully remove the Doppler effect as waves of different frequency travel at different speeds, it is good enough to help with clarity of comparison.

Force measurements are shifted vertically by the different mean forces from different current speeds – see figure 5(*e,f*). This mean force in current only, shown as horizontal dashed lines in figure 6(*a,b*) and as dots in figure 6(*c*), scales linearly with $u_c|u_c|$, confirming the appropriateness of the Morison drag form used in simple current blockage. This simple current blockage force (equations 7 and 8 in Taylor 1991) is

$$F_{\text{current only}} = \frac{1}{2}\rho\, C_d\, A\, u_{scb}^2,$$
$$\text{where } u_{scb} = u_c \left(\frac{1}{1 + \dfrac{C_d A}{4 A_f}} \right). \tag{4.1}$$

https://doi.org/10.1017/jfm.2025.180 Published online by Cambridge University Press

The drag coefficient inferred from measurements is $C_d = 0.7$, $A = 1.12$ m^2 is the summed solid area of all structural members normal to the incident flow, and $A_f = 0.55$ m^2 is the frontal area bounding the entire structure. A vaue of C_d of 0.7 is a plausible number at laboratory scale on smooth cylinders at relatively high Reynolds number ($Re = ud/\nu \approx 10^4$ near the mean free surface, where u is the total fluid velocity and ν is the kinematic fluid viscosity). Note that we do not need C_d to estimate wave-current blockage effects, only the measured forces with and without current (see § 2). As this paper is concerned with the force behaviour in combined waves and current, we removed this current-only force from the measured force, as shown in figure 6(*a,b*). This current-only force is revisited in § 5.3.

Error waves are freely propagating waves spuriously generated by a wavemaker when low-order wavemaker theory is used for motion control. Moreover, reflections off the beach represent an additional source of potential contamination of measurements. For our tests, second- and higher-order error waves could be present as the wavemakers were run without second-order correction (Schäffer 1996). To check for potential contamination, we analysed data from three fixed wave probes, which measured the free surface at different positions in the tank – see figure 7(*a*) for their positions and figure 7(*b*) for the free surface measurements. The free surface measurements have been separated into their frequency harmonics using the two-phase combination method (5.1) (see § 3*a* of Fitzgerald *et al.* 2014). The scale of the vertical free surface disturbance is captured by the left-hand vertical axes, and the horizontal position of the measurement point along the tank is represented by the right-hand vertical axes. Figure 7(*b i*) (i.e. the linear signal) shows the main focused wave group evolving in time and space; it is generated at the wavemakers at $t = -21$ s, propagates along the flume at the linear group velocity (represented by the lines) and reaches the beach at approximately $t = 20$ s. All other free surface harmonics (figure 7*b ii–iv*) have bound wave components that propagate with the focused wave group, but they also have free error waves released from the wavemaker. These free error waves propagate at different speeds to the main focused wave group: the (2−) error wave (represented by the -- lines) travels faster, at the shallow water phase speed, while the (2+) and (3+) error waves travel slower. The mathematical expressions for each of these propagation speeds is given in the caption of figure 7. Near the point of wave focus at the longitudinal centre of the tank (represented by the — line) at $t = 0$, the error waves propagating from the wavemakers do not contaminate measurements: the (2−) error wave arrives well before $t = 0$ and the (2+) and (3+) error waves arrive long after. However, we estimate that the (2−) error wave reflected off the beach arrives back at the tank centre $t \approx 1.5$ s after wave focus, which would contaminate the second half of the (2−) force measurements. Although the free surface disturbance from this (2−) error wave is very small (largely undetectable in figure 7*b ii*), it may be associated with more considerable wave kinematics which would have a measurable effect on force. We also note that towing the carriage to represent current has only a small effect on the arrival time of the reflected (2−) error wave (arrival time only changes by ~ 0.2 s between the fastest negative and positive currents), as the speed of the carriage is much slower than the error wave propagation speed. So in summary, the focused wave group measurements have minimal contamination from error waves, except for perhaps part of the (2−) force measurements. This relatively clean experiment is made possible by using focused wave groups, which allow an extreme wave to be tested deterministically and over a short time frame.

To analyse free surface and force harmonics, it is instructive to transform the crest- and trough-focused time series into power spectra in the frequency domain. Smoothed spectra in figure 8 were produced using a 4-point moving average, equivalent to a window

https://doi.org/10.1017/jfm.2025.180 Published online by Cambridge University Press

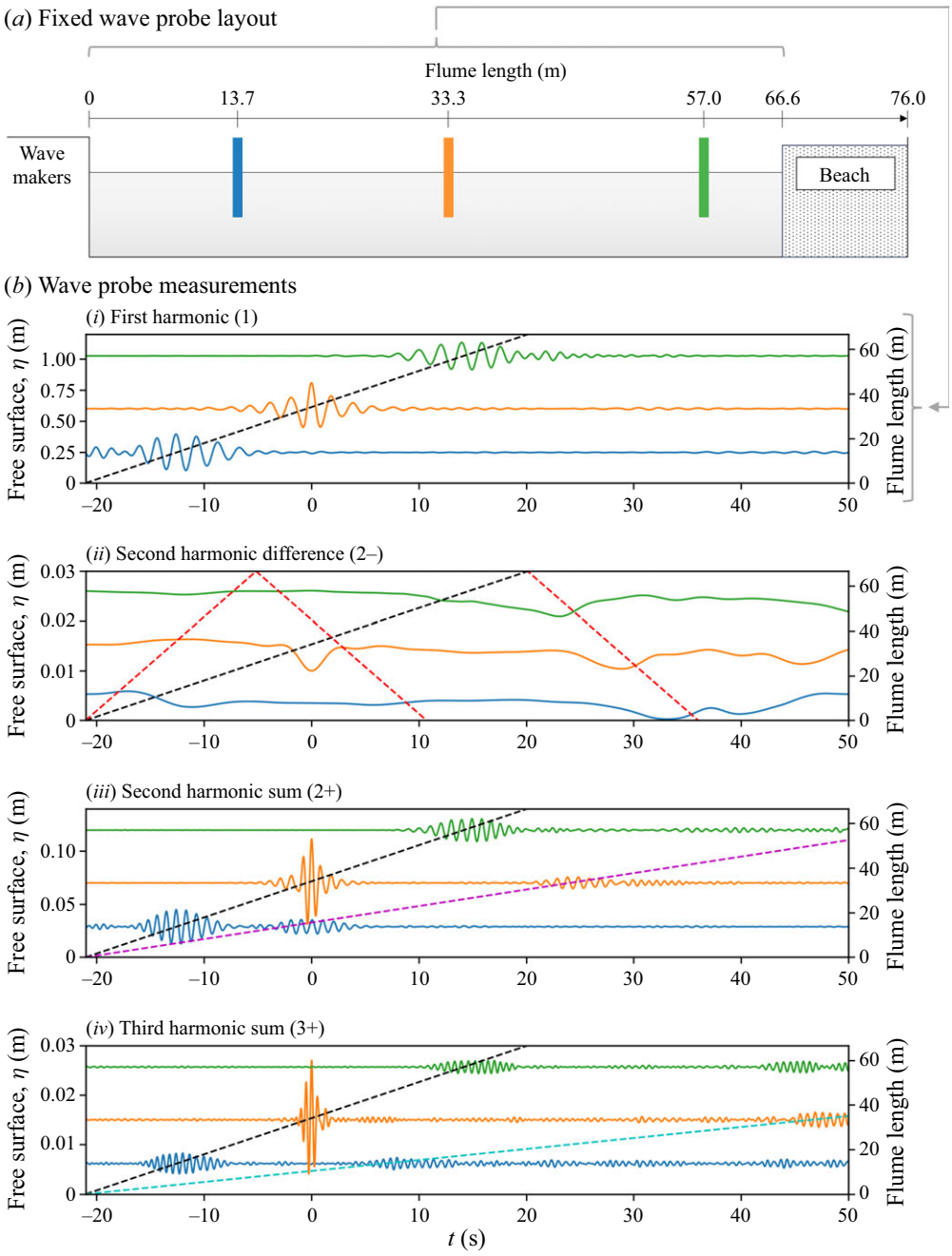

Figure 7. Three fixed wave probes measured the undisturbed free surface (i.e. without the jacket) at different positions along the tank: (—) at the wave focus location at the longitudinal tank centre, (—) closer to the wavemaker and (—) closer to the beach. Their positions are shown in (*a*), and the measured time histories of the free surface harmonics (obtained using the two-phase combination method (5.1)) are shown in (*b*). The dashed lines represent the propagation speed of different wave packets: (– –) c_g, f_p, (– –) $c_{shallow}$, (– –) c_g, $2f_p$ and (– –) $c_{g,3f_p}$, where $c_{shallow} = \sqrt{gh}$ is the shallow water phase speed, and $c_g = \omega/k(1/2 + kh/\sinh(2kh))$ is the group velocity at different multiples of the peak frequency f_p.

https://doi.org/10.1017/jfm.2025.180 Published online by Cambridge University Press

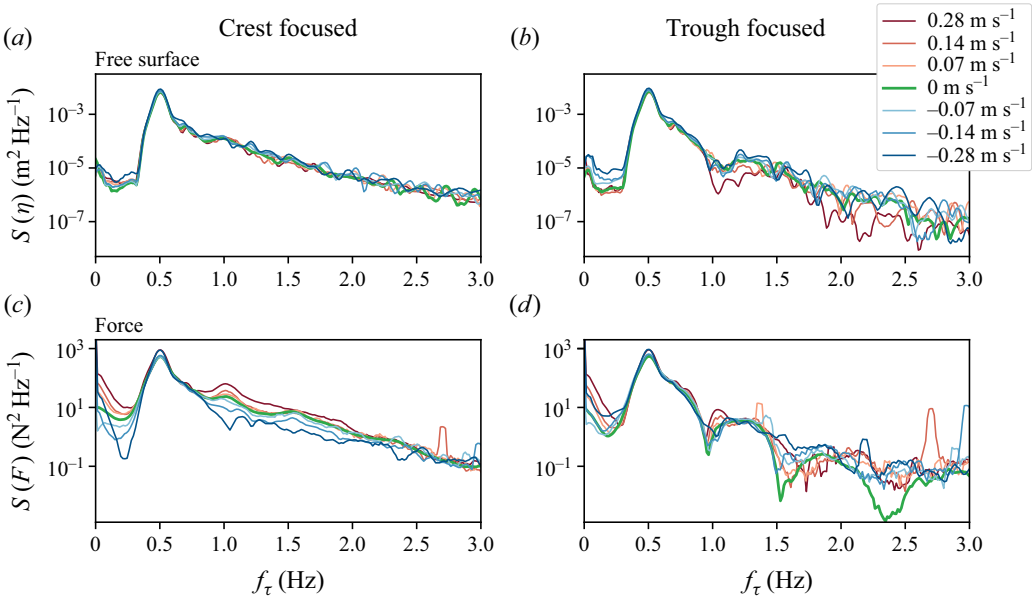

Figure 8. Measured free surface variance density spectra $S(\eta)$ recorded by the carriage-mounted wave probe (top panels) and total force variance density spectra $S(F)$ for (*a,c*) crest-focused wave groups and (*b,d*) trough-focused wave groups, with different current speeds. The frequency axis f_τ relates to the Doppler-scaled time τ.

of ~ 0.05 Hz. Crest-focused force power spectra (figure 8*c*) are sorted by current speed at frequencies near 1 Hz (at $\sim 2\times$ the linear frequency), indicating a dependency with current, while trough-focused spectra (figure 8*d*) show a partial cancellation close to 1 Hz for all current speeds. We concentrated our analysis on the first three harmonics (so 2−, 1, 2+, 3+) with frequency ranges up to ~ 2 Hz, which give good signal-to-noise ratios and are the most relevant for the design of offshore structures.

The first longitudinal mode of vibration of the jacket on its support is at 5.5 Hz, as confirmed by a dynamic push test. Although this is $\sim 10\times$ the peak wave frequency, we expect that this mode of structural vibration gives some force amplification effects for the frequency range of interest. Assuming a simple mass-spring-damper system with a damping ratio of 0.09 (estimated from the dynamic push test data), we estimate that forces at 2 Hz are amplified by roughly 15 %, but forces at the peak wave frequencies are amplified by less than 1%. This possible small force amplification does not impact the analysis of wave-current blockage effects, which, as described in the following sections, relies on the relative difference between measured forces with and without current, rather than on their absolute values. We note that changes in wave encounter frequency caused by towing the carriage have negligible impact in this respect, with differences in estimated force amplifications between tests with no current and with the fastest currents being (at most) 2 % at higher frequencies, and negligible nearer to the peak wave frequency.

To summarise, we have shown that the experimental results are highly repeatable, with minimal contamination from free error waves (besides perhaps for the latest part of the (2−) force time history). Structural vibration may cause small amplifications in measured forces at higher frequencies near 2 Hz, but we do not expect this to affect the analysis of blockage effects. In the next section, we analyse the data further to investigate the behaviour at different frequency harmonics, the relative contribution of Morison drag and inertia forces and wave-current blockage effects.

https://doi.org/10.1017/jfm.2025.180 Published online by Cambridge University Press

5. Force harmonics results and discussion

5.1. *Harmonic decomposition of total force*

To decompose the free surface and force time histories into their linear and higher harmonics, we used the two-phase combination method (Fitzgerald *et al.* 2014), which combines the crest-focused time series F_{0° and the trough-focused time series F_{180° to separate odd and even harmonics

$$\begin{aligned} \text{Odd harmonics} &= \frac{1}{2}(F_{0^\circ} - F_{180^\circ}) \\ \text{Even harmonics} &= \frac{1}{2}(F_{0^\circ} + F_{180^\circ}). \end{aligned} \tag{5.1}$$

Note that (5.1) defines the odd and even force harmonics, but the same formula applies for free surface. After applying (5.1), the first three harmonics were separated from other odd or even harmonics by digital filtering, where the frequency bands for each harmonic were estimated by Stokes wave theory (see appendix A of Walker *et al.* 2004), and then manually adjusted to both maximise the spectral energy within the frequency band and minimise the spectral energy in adjacent harmonics. The resulting free surface and force harmonic time series are shown in figure 9. The odd and even terms of the first three harmonics are well separated in frequency, so we are confident that the two-phase combination method extracts the harmonics with good accuracy.

To independently analyse the effect of current on drag loads, the tested wave must be similar for all current speeds. We assessed this similarity by comparing free surface harmonic time series – see left panels of figure 9. The linear free surface is very similar for all current speeds. There are differences in higher free surface harmonics, which could be caused by the spatial and temporal differences in the position of the jacket or from experimental variability, but these differences are small (note the small vertical axis scales). The (2−) terms show a free surface set down as the focused wave group passes through, which is reasonably consistent with second-order wave theory (e.g. Dalzell 1999). Overall, we conclude that the encountered wave forms are similar for all current speeds.

Forces (figure 9, see right panels) are highly nonlinear; while the amplitudes of higher free surface harmonics are collectively (i.e. (2−) + (2+) + (3+)) roughly 25 % of the linear free surface amplitude, higher harmonic force amplitudes are collectively up to 85 % of the linear force amplitude, hence emphasising their importance for jacket design. Linear forces show a small dependency with current, with the fastest positive current speed of 0.28 $\mathrm{m\,s^{-1}}$ represented by the right hand having a notably higher peak force. Similar to the linear forces, the amplitudes of the (3+) forces have little variation with current, with only the higher negative current speeds having reduced amplitudes near the focused peak. In contrast to these odd harmonics, the amplitudes of the even (2−) and (2+) terms are highly dependent on current and are neatly sorted; the largest negative current speed gives the smallest amplitude and the largest positive current speed gives the largest amplitude. This general behaviour is predicted by the drag force harmonic expressions in table 2.

The force harmonics shown in figure 9 are the total force, so in a Morison-type force approximation the harmonics contain both drag and inertia force components. In this approximation, drag forces are symmetric about wave crests, while inertia forces are 90° phase shifted ahead of wave crests and so are skew symmetric (positive first, then negative, wave by wave). The exception to this rule is the (2−) inertia force, which will also be close to skew symmetric but will be negative first, being mostly driven by the acceleration of the (2−) return flow beneath the wave group. The (2−) forces also vary on the time scale of

https://doi.org/10.1017/jfm.2025.180 Published online by Cambridge University Press

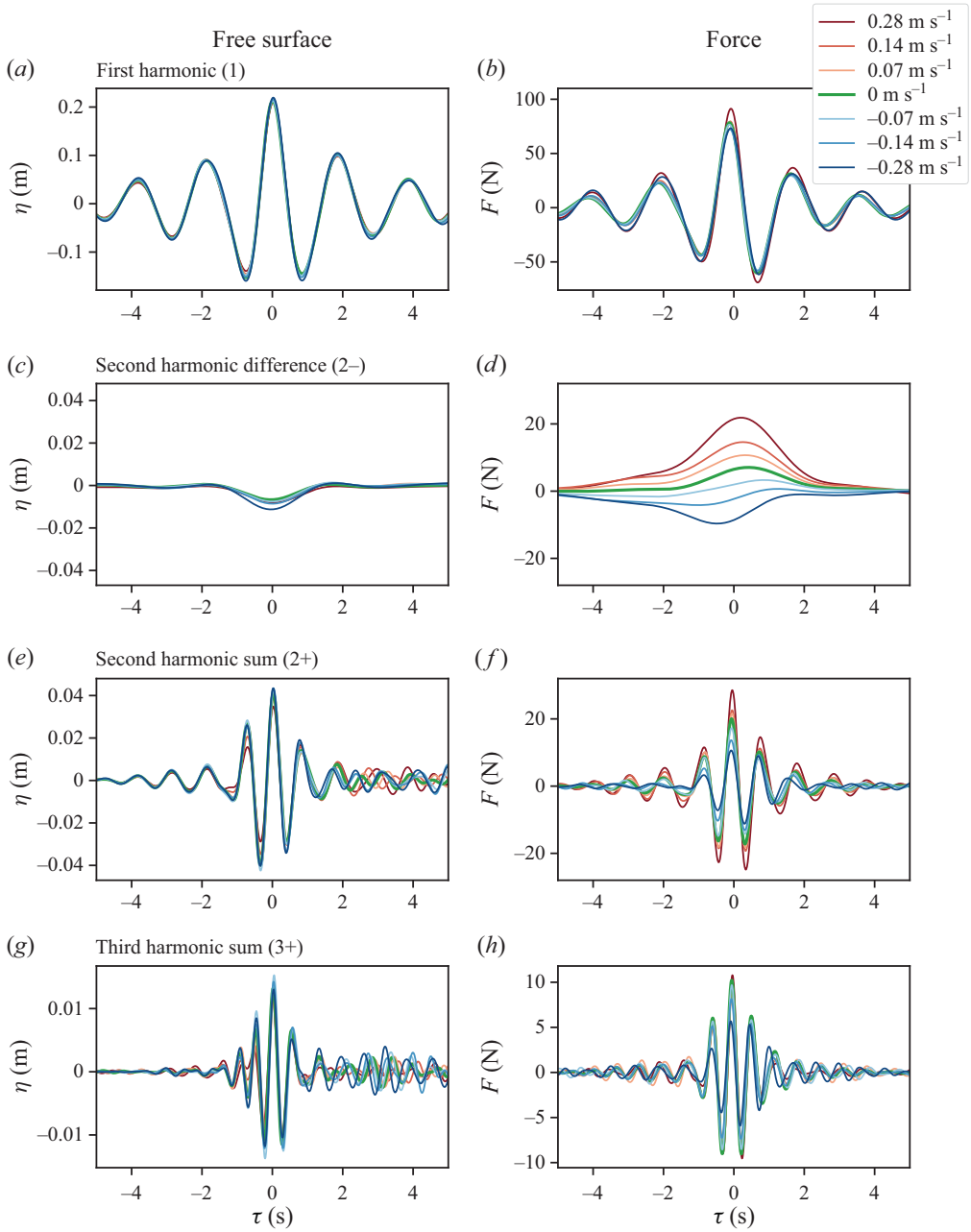

Figure 9. Harmonic time series of free surface recorded by the carriage-mounted wave probe (left panels) and total force (right panels). The mean drag force from current has been removed from the (2−) force (*d*) for clarity of comparison.

the wave group envelope, not wave by wave. Applying these symmetry arguments to the force harmonics in figure 9, it can be seen that the (1), (2+) and (3+) forces are roughly symmetric about the free surface peak at $\tau = 0$, which suggests they are drag dominated. In contrast, the (2−) force is asymmetric; forces vary with the envelope of the wave group, but the forces measured well before the focused peak are larger than the forces the same

https://doi.org/10.1017/jfm.2025.180 Published online by Cambridge University Press

time after. This asymmetric shape is opposite to the theoretical shape of the (2−) inertia term, which is negative before the focused peak and positive after. Logically, if this inertia term could be removed, the asymmetry would only increase in severity, suggesting that the (2−) force is also drag dominated. We assume the asymmetry is a drag-related fluid memory effect, where the viscous flow generated from past wave loading events persists over a period of time and affects the drag forces from future wave loads. Unfortunately, the (2−) forces measured after $\tau = 0$ may be contaminated by an error wave (see figure 7(*bii*)), which may contribute to this asymmetry and explain why the peak of the (2−) force with zero current occurs slightly after the focused peak. As the effect from the error wave cannot be isolated, we cannot comment more on the presumed asymmetric drag behaviour, but note that it could be a topic of further study.

Although the measured forces appear to be mostly drag, inertia forces will still make a small contribution to the peak measured forces. To apply the wave-current blockage theory developed in § 2 (which only applies to drag forces), it is important to separate the drag and inertia forces. Next, we will attempt to separate these force components through a symmetry/skew-symmetry argument.

5.2. *Harmonic decomposition of drag and inertia forces*

To separate drag and inertia force components, we used a method proposed by Santo *et al.* (2014), which relies on symmetry about wave crests and assumes that drag forces are in phase with crests and inertia forces are 90° phase shifted (which is consistent with a Morison-based force approximation). The method combines the total force $F(t)$ and its time-reversed signal $F(-t)$ to give

$$\begin{aligned} \text{Drag} &= \frac{1}{2}(F(t) + F(-t)) \\ \text{Inertia} &= \frac{1}{2}(F(t) - F(-t)). \end{aligned} \tag{5.2}$$

This method assumes the free surface is symmetrical about $t = 0$, which is approximately true for both crest- and trough-focused wave groups – see figure 5. Nonlinear inertia contributions share the same skew-symmetric shape around the focused peak as linear inertia, so the drag/inertia separation method should hold for most higher force harmonics. The one important exception to this is the (2−) force, which may have some asymmetric drag loading and hence is not compatible with these symmetry arguments.

After applying the drag and inertia separation method, we then applied the same two-phase decomposition method (5.1) and subsequent digital filtering to isolate each drag and inertia force harmonic. The results are shown in figure 10. Although the (2−) force separation may not be valid, we chose to show these results as they give a rough indication of the small contributions from inertia relative to drag. For the (1), (2+) and (3+) forces, the separation of drag and inertia terms appears to work well. As expected, the drag components are comparatively larger (peak first harmonic drag is $\sim 2 \times$ peak linear inertia), and they contain most of the effects from current.

Now that we have removed the inertia component from the measured force, we can apply the theory developed in § 2 to the isolated drag forces and hence estimate wave-current blockage effects. This is discussed in § 5.3.

5.2.1. *A brief aside on the dependency of inertia forces with current*

Although this paper is mostly concerned with the effects of current on drag forces, inertia forces are also affected. The linear inertia forces in figure 10(*b*) show that more positive

https://doi.org/10.1017/jfm.2025.180 Published online by Cambridge University Press

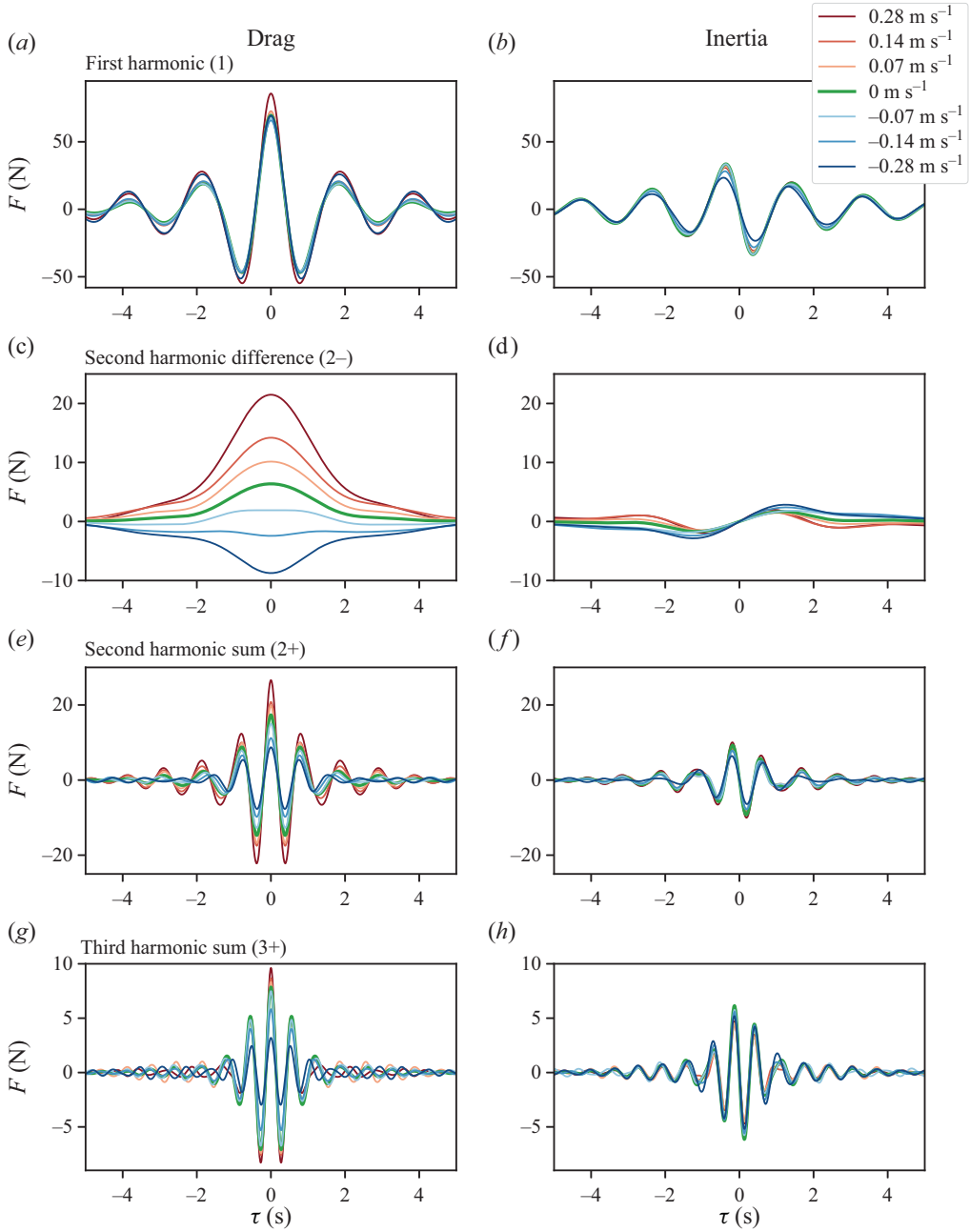

Figure 10. Force harmonic time series of drag (left panels) and inertia (right panels). The labels of the (2−) forces are coloured red to indicate that we expect the drag/inertia separation method (5.2) to be less appropriate.

currents generally give larger peak forces. To understand this dependency, we consider the complete inertia term for slender cylinders, including the convective derivative terms from the higher-order FNV model (Kristiansen & Faltinsen 2017) that were initially ignored in the Morison equation (1.1). This complete inertia term is

https://doi.org/10.1017/jfm.2025.180 Published online by Cambridge University Press

$$\text{Inertia} = (\cdots)\left(2\frac{\partial u}{\partial t} + u\frac{\partial u}{\partial x} + 2w\frac{\partial u}{\partial z}\right), \tag{5.3}$$

where (u, w) are the horizontal (x-direction) and vertical (z-direction) total fluid velocity. The total horizontal fluid velocity u includes the fluid velocity from both waves and current, so $u = u_w + u_{cs}$. The effect of current on inertia is two fold.

- On the $\partial u/\partial t$ term: the Doppler-shift effect caused by the carriage moving at the undisturbed current speed u_c acts to scale the measured time t by $(1 + u_c/c)$. This also has the effect of linearly scaling the $\partial u/\partial t$ inertia term by the same factor.
- On the convective derivative terms, $u\partial u/\partial x + 2w\partial u/\partial z$: substituting $u = u_w + u_{cs}$ simplifies to $u_{cs}\partial u_w/\partial x$, as $w\partial u/\partial z$ is unaffected by depth-uniform current and as the wave contributions of each term roughly cancel each other out (as shown by Taylor *et al.* (2024)). The resulting $u_{cs}\partial u_w/\partial x$ relates to the blocked current u_{cs} and acts to decrease inertia forces with an increasingly positive current (as $\partial u_w/\partial x$ is proportional to $-\partial u_w/\partial t$).

To summarise, there is some effect of current on the inertia term linearly, but these effects are small (figure 10*b*) so we did not analyse these further. Importantly, all inertia force components with current still have the same skew-symmetric shape around the focused peak, so the method of separating drag and inertia forces (5.2) remains valid.

Finally, we remark that the fully nonlinear inertia forces with zero current could be estimated using the Transformed-FNV model (Taylor *et al.* 2024) which requires knowledge of only the linear free surface at the jacket. However, this model assumes the jacket occupies the entire water column, which ours does not, and it cannot (yet) explain the effects of current. Future work to extend the Transformed-FNV model to include current would be of value.

5.3. *Estimating wave-current blockage effects in large waves*

We now discuss the principal objective of this paper, to estimate the reduction in the blocked current u_{cs} from the undisturbed current u_c, at the point in time that corresponds to the peak force on the structure (i.e. at $t = \tau = 0$ s). This is key for structural engineers looking to design or re-assess real jacket structures. Recall that the expressions for drag force harmonics given in table 2 show that the force with current is equal to a pure wave force term $\times$ a multiplier which depends on u_{cs}. Hence, u_{cs} can be estimated from accurate force measurements with and without current, and the extent to which u_{cs} is reduced from the undisturbed current speed indicates the magnitude of wave-current blockage effects. Importantly, the drag force harmonic expressions only apply to fluid loading regimes where u_{cs} is small compared with the wave-driven fluid velocity u_w, so for extreme waves where $u_w \gg u_{cs}$ for the majority of the water column. The tested focused wave groups give an extreme wave crest (or trough) at $\tau = 0$, hence the drag force harmonic expressions in table 4 (which have been adjusted from the expressions in table 2 to account for the jacket not reaching the tank floor) can be applied to the measured drag forces at this point in time.

While the (1), (2−), (2+) and (3+) drag force measurements could all be used to estimate u_{cs}, the (2+) measurements are arguably the most suitable given that they give good separation in peak forces with current. The (2−) measurements also give good force separation with current, but are complicated by drag asymmetry, possible error wave contamination and other factors like the second-order return flow under the focused wave group which have not been accounted for. Because odd force harmonics (1) and (3+) have smaller amplification from current, their peak forces are not as well separated for

https://doi.org/10.1017/jfm.2025.180 Published online by Cambridge University Press

Undisturbed current ($\mathrm{m\,s^{-1}}$)	Estimated u_{cs} ($\mathrm{m\,s^{-1}}$) From (2+)	From (2−)	From (1)	**Average**	Simple current blockage (u_{scb})
0.280	0.065	0.16	0.107	**0.11**	0.21
0.140	0.024	0.083	0.029	**0.045**	0.10
0.070	0.017	0.040	0.025	**0.027**	0.052
−0.070	−0.017	−0.048	−0.025	**−0.030**	−0.052
−0.140	−0.043	−0.094	−0.075	**−0.071**	−0.10
−0.280	−0.061	−0.161	−0.148	**−0.12**	−0.21

Table 3. Estimates of the blocked current, u_{cs}, using the peak measured (2+), (2−) and (1) drag forces in figure 10*(a,c,e)* with the corresponding expressions in table 4. The average of these values are compared with an estimate for u_{cs} using the simple current blockage model (4.1). Note that, although we give some of these estimates to three significant figures, we do not claim this level of accuracy, rather this is done to minimise rounding errors when calculating averages.

different currents, hence any errors in experimental variability and in the separation of drag and inertia forces would translate to larger errors in the estimates of u_{cs}. Despite these difficulties, we chose to use (1), (2−) and (2+) drag forces, only discarding the (3+) measurements as the peak forces with positive currents are not well separated and would hence introduce unacceptably large errors. To estimate u_{cs} for each undisturbed current speed, we substituted the measured peak drag forces into the expressions in table 4 and solved for u_{cs} – the results are presented in table 3. The additional parameters of the wave frequency ω and wave amplitude a (and hence the wavenumber k and phase speed c), were estimated from the spectral peak period of the linear free surface with $0\,\mathrm{m\,s^{-1}}$ current, giving $\omega = 3.3\ \mathrm{rad\,s^{-1}}$ and $a = 0.21$ m. It is important to note that the choice of wave period is somewhat arbitrary, and it could be argued that, as we are interpreting irregular waves with a regular wave model, choosing a wave period closer to the zero-upcrossing period T_z is more appropriate than the peak period T_p. If instead of using T_p we used $0.9T_p$ (which is closer to T_z), the average u_{cs} estimates in table 3 increase by $\sim 20\,\%$ (i.e. from $0.11\,\mathrm{m\,s^{-1}}$ to $0.13\,\mathrm{m\,s^{-1}}$ for a $0.28\,\mathrm{m\,s^{-1}}$ undisturbed current). So, while the estimates are sensitive to the choice of wave period, this sensitivity does not change the trend in results.

The estimates for u_{cs} using the (2+), (2−) and (1) drag forces presented in table 3 are all considerably lower than both the undisturbed current speed and estimates using the industry-standard simple current blockage model (4.1). The estimates vary between drag force harmonics: (2+) give the lowest estimates that are consistently $\sim 20\,\%$ of the undisturbed current, (2−) give consistently higher estimates (but we believe the structure of these forces are more complex than our derived (2−) expression assumes) and (1) give estimates in between (2+) and (2−) but with more variability (presumably due to larger errors). Despite this variability, the important indication of new physics is that all estimates of u_{cs} are considerably smaller than the undisturbed and the simple blocked current. These simple blocked current estimates were validated by Archer *et al.* (2024*b*) for the same jacket model in current-only tests (no waves). We therefore conclude that the extra reduction in the blocked current that we estimate from our experiments can only come from the addition of the large wave group. This demonstrates a strong wave-current blockage effect as large waves pass through the structure. It is perhaps surprising that this extra blockage occurs over relatively fast time scales associated with the compact wave group – see the last paragraph in § 5.4 for further discussion on this. We contrast this

https://doi.org/10.1017/jfm.2025.180 Published online by Cambridge University Press

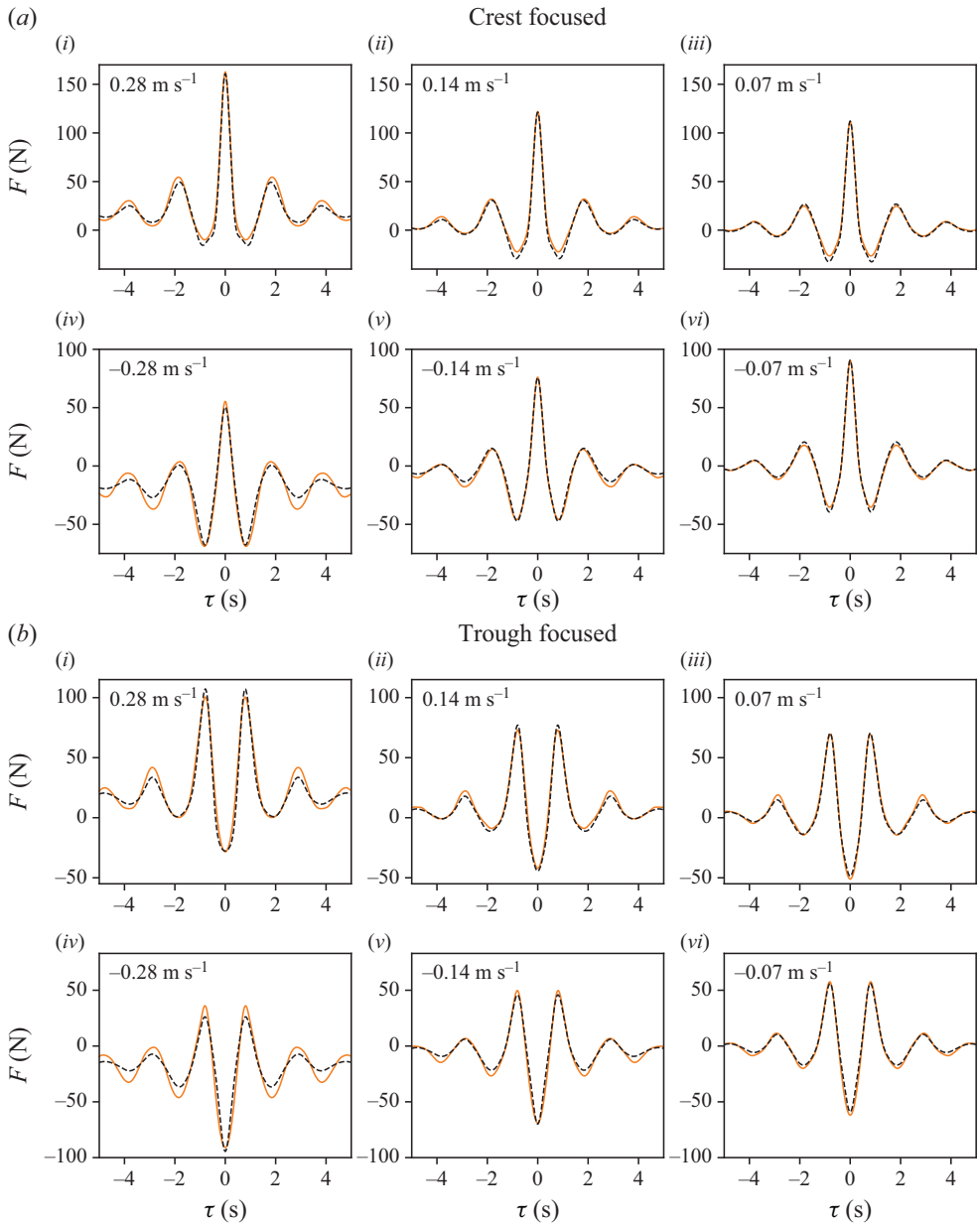

Figure 11. Measured (——) and reconstructed (– –) drag force time histories for (*a*) crest-focused and (*b*) trough-focused wave groups with different undisturbed current speeds using the expressions in table 4 (valid for $u_w \gg u_{cs}$) together with the average u_{cs} estimates from table 3.

reduction in current speed to the wave kinematics – the recent measurements reported in Archer *et al.* (2024*b*) show that the wave kinematics are essentially undisturbed by the presence of the structure, i.e. are not blocked.

To crudely estimate u_{cs} for each current speed, the estimates using the (2+), (2−) and (1) drag forces were averaged – see table 3. These averaged estimates are all roughly 40 % of the undisturbed speed, and are approximately half of the simple blocked currents. In Appendix D, we estimate u_{cs} using a different lighter-weight jacket (figure 15*a*), formed

https://doi.org/10.1017/jfm.2025.180 Published online by Cambridge University Press

by removing the array of 24 vertical conductors from the structure. This analysis indicates that even for a structure that is much less structurally dense, u_{cs} is still substantially reduced, in this case to $\sim 50\,\%$ of the undisturbed current. To validate the appropriateness of averaging the u_{cs} estimates from (2+), (2−) and (1) drag forces, we reconstructed the force time histories using these averaged estimates and compared them with measured drag forces. To reconstruct the drag forces, the wave-only drag force measurements (which provide the necessary phase information) are scaled by the [multiplier] expressions in table 4, substituting the averaged u_{cs} estimates in table 3. The resulting forces, shown in figure 11, are in good agreement with one another at the peak crest/trough. The agreement between the reconstructed and measured drag forces gets worse for times either side of the focused peak, which is to be expected as the drag force harmonic expressions only apply around $\tau = 0$ where wave velocities are much larger than current. Moreover, reconstructing the full force time history is a more difficult problem as the blocked current u_{cs}, the wave amplitude a, and to a lesser extent the wave frequency ω, all vary in time – this is discussed more in § 5.4. To match the vertical shift in forces, we had to add back in the mean force from current only (the force which was removed in figure 6 and which is described by simple current blockage). Although the expressions in table 4 are meant to describe the total drag force (and hence the current-only force should not need to be added at $\tau = 0$), the expressions assume u_{cs} is constant with depth, where in fact it increases with depth as u_w decays. At depths where u_{cs} is not small relative to u_w the expressions are no longer valid, and the mean current-only force dominates. This effect is only significant for the largest $\pm 0.28\ \mathrm{m\,s^{-1}}$ currents (which represent an extreme $2.5\ \mathrm{m\,s^{-1}}$ current at full scale). Despite these complexities, the good agreement between measured and reconstructed forces at the peak crest/trough indicates that averaging the u_{cs} estimates from the (2+), (2−) and (1) drag forces is reasonable.

The good agreement between measured and reconstructed drag forces in figure 11 also shows that, despite the scatter in u_{cs} estimates in table 3, our method captures the bulk physics of the problem. Coupled with the demonstrated accuracy of the method with Stokes' fifth-order waves (Appendix B), this agreement shows that our method is valid for engineering analysis. Importantly, this claim of validity does not imply that the average u_{cs} estimates in table 3 accurately capture the actual current speeds throughout a jacket structure – the actual flow structure is far more complex, varying significantly around each structural member and with depth. For engineering analysis of structural forces, however, resolving this actual flow structure is unnecessary. For this purpose, the fact that the u_{cs} estimates give the correct force time histories when fed into a Morison force model demonstrates the validity of the method. To further substantiate this argument, we note that the results are in qualitative agreement with a parallel set of experiments in Archer *et al.* (2024*b*), which directly measured (using acoustic Doppler velocimeters) large reductions in current for combined wave and current tests. Unfortunately, the data in Archer *et al.* (2024*b*) cannot be directly compared with the results here, as the same focused wave groups were not tested (because the instrumentation and seeding did not permit acoustic Doppler velocimeter measurements in the large wave tests reported here), and the blocked current u_{cs} was not measured (only the flow speeds up-wave and down-wave of the jacket). Nonetheless, as the results in this paper and in Archer *et al.* (2024*b*) demonstrate wave-current blockage effects using two entirely different approaches, based on measured forces and flow velocity respectively, it strongly suggests that these physical effects are real. Furthermore, the effects are of practical significance, as they translate to substantial reductions in peak force estimates (see figure 13*a*), which should be considered in the design and re-assessment of offshore jackets.

https://doi.org/10.1017/jfm.2025.180 Published online by Cambridge University Press

To summarise, we have estimated that, for the tested jacket structure and wave condition, the blocked currents are roughly 40 % of the undisturbed speed at the point in time that corresponds to the peak force. While different jacket geometry and wave conditions will yield different reductions in current, our method to estimate this reduction may be generally valid for all jacket-type structures subjected to a current and high KC number oscillatory flows. In future work, we will expand this analysis to more test cases using computational fluid dynamics simulations, which will involve fully nonlinear three-dimensional wave kinematics and will represent jacket structures as porous blocks (as in Santo *et al.* 2015, 2018*b*). These simulations will serve as further validation of the analytical model described in this paper, and give insight into the possibility of deriving a generalised adjustment factor that reduces the simple blocked current to account for the extra blockage effect from waves.

In this section, we have concentrated analysis on the point in time that corresponds to the peak force. While this is most important for structural design, from a fundamental viewpoint we also wanted to find a suitable form that can reconstruct the entire force time history. This is discussed next.

5.4. *Estimating the time-varying effects of combined waves and blocked current*

The blocked current u_{cs} has been estimated at two regions, one at the focused wave peak at $\tau = 0$ where it is the most reduced (which we now denote as u_{full}), and one far away from the focused peak where there are no waves and only current, for which it is given by the simple current blockage model (Taylor 1991) and is the least reduced (calculated with (4.1) and denoted u_{scb}). See table 3 for these estimates at each current speed. Between these two regions, u_{cs} is unknown but we hypothesise that its variation in time may be related to the linear wave envelope, i.e.

$$u_{cs}(\tau) = u_{scb} - (u_{scb} - u_{full}) \left(\frac{a(\tau)}{\max(a(\tau))} \right)^p , \tag{5.4}$$

where $a(\tau) = (\eta_1^2 + \eta_{1H}^2)^{1/2}$ is the linear wave envelope where η_1 is the linear free surface and η_{1H} its Hilbert transform (i.e. the harmonic conjugate of η_1), and p is an adjustable parameter which dilates the wave envelope.

For standard engineering force calculations where the full Morison form is used, the blocked current in the form of (5.4) (if valid) can be added to wave kinematics (which are estimated from another model, e.g. Stokes' 5th (Fenton 1990)) to give the total local flow velocities and hence give the total force time history. However, for our analysis where we use the approximation of Morison drag (2.2) to decompose frequency harmonics, the total drag force time history cannot be captured as simply. This is because the drag force harmonic expressions in table 4 are only valid near $\tau = 0$ around the centre of the large group, where wave kinematics are much larger than current (i.e. $u_w \gg u_{cs}$). Near the tails of the focused wave group where waves are much smaller (i.e. $u_w < u_{cs}$), Morison drag can be expanded as $\mathrm{sgn}(u_{cs}) \times (u_w^2 + 2u_w u_{cs} + u_{cs}^2)$, and different drag force harmonic expressions apply. These are derived in Appendix C using the same method as in § 2. As waves are small, only two terms in these new expressions are non-negligible, the linear wave × current term (C3) and the (2−) current × current term ((C5), giving $F_{\text{current only}}$). The other terms, (C1), (C2), (C4) and (C6), are neglected. The total drag force in this small wave regime can be approximated as

$$F = F_{\text{current only}} \left(1 + \frac{2D_E}{\alpha h} \beta^2 \, \eta_1 \left(\frac{u_{cs}}{c} \right)^{-1} \right) , \tag{5.5}$$

https://doi.org/10.1017/jfm.2025.180 Published online by Cambridge University Press

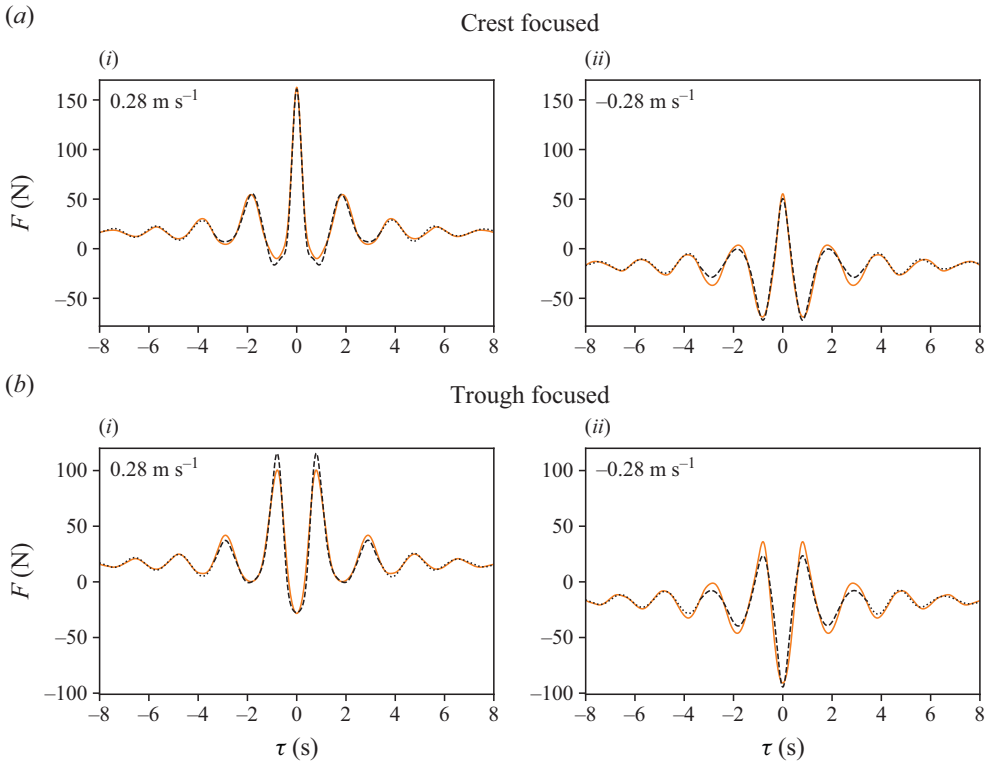

Figure 12. Reconstructed drag force time histories using a switching model, using the $u_w \gg u_{cs}$ expressions in table 4 when waves are big (– –) and the $u_w < u_{cs}$ expression (5.5) when waves are small (····). These two models are switched at the free surface zero-crossing near $\tau = 3.5$ s either side of the focused peak. These reconstructed forces are compared with measured drag forces (—).

where $\beta = u_{cs}/u_{scb}$ is the ratio between the blocked current and the simple blocked current given by (4.1), αh is the depth of the jacket in our experiments, $D_E = 1 - \sinh(kh(1-\alpha))/\sinh(kh)$ and η_1 is the linearised free surface.

We now have two drag force models, one that applies in regions where $u_w \gg u_{cs}$, and one that applies where $u_w < u_{cs}$. The force time histories can therefore be reconstructed with a switching model, using the $u_w \gg u_{cs}$ expressions where waves are big and using the $u_w < u_{cs}$ expressions where waves are small. Figure 12 compares measured drag forces with the reconstructed forces using the switching model. Only the fastest ± 0.28 m s^{-1} currents are shown as these give the largest scaling with current and hence are the most interesting test cases. These reconstructed forces are evaluated using the time-varying u_{cs} profile described by (5.4), with $p = 1$ giving the best fit to measured forces (which suggests that the variation in u_{cs} matches the wave envelope). The other parameters a, ω and k are held constant in time, a being the peak of the linear wave envelope, and ω and k given by the peak wave frequency. The agreement between reconstructed and measured drag forces are very good at the peak wave crest/trough at $-0.5 < \tau < 0.5$, and are also good at $\tau < -3.5$ and $\tau > 3.5$ where waves are small compared with current. In between these regions (where we reconstruct the force assuming $u_w \gg u_{cs}$), the agreement is poorer, which is presumably because this region is transitional between $u_w \gg u_{cs}$ and $u_w < u_{cs}$ regimes and hence neither drag force model is valid. Analytical drag force expressions cannot be defined for these transitional regions. Despite this, the general behaviour is

https://doi.org/10.1017/jfm.2025.180 Published online by Cambridge University Press

still captured well for the total drag force time histories. We again emphasise the good agreement at the large wave crest/trough at $\tau = 0$, which is of primary importance for structural design.

The good agreement between total force time histories supports the hypothesised time variation of u_{cs} in (5.4), and fitting $p = 1$ suggests that the variation in u_{cs} matches the wave envelope. This empirical result poses the question of why, from a fundamental fluid mechanics perspective, the blocked current might vary with the wave envelope, and why this variation occurs on such fast time scales (associated with the compact wave group). To begin to answer this question, we recall the wave $\times$ current drag force term, $2|u_w|u_{cs}$ in (2.2), which is dominated by (2−) and (2+) frequency harmonic contributions. For the slowly varying (2−) term, u_w scales with the wave envelope $a(\tau)$, hence the dominant (2−) drag forcing is $\sim a(\tau)u_{cs}$. This force on the structure, which (we assume) arises close to instantaneously on overall timescales because the KC number is always high, has an equal and opposite reaction force on the fluid in the upstream direction. This fluid force acts as a distributed force dipole and creates an upstream flow, which one may interpret as a local reduction in the incoming (downstream) current, hence leading to current blockage. This fluid force dipole, although arising from drag forces, has a global potential flow effect, so can be assumed to act instantaneously on the flow field (as all boundary effects do in potential flow problems). So, as the fluid force scales with the wave envelope, it follows that the blocked current u_{cs} also instantaneously varies with the wave envelope, hence justifying the form of (5.4) with $p = 1$. Finally, note that although we only tested compact wave groups, if the variation in u_{cs} given by (5.4) is generally applicable, the consequences for random wave fields are quite striking – the blocked current will be continuously more reduced (or more blocked) compared with the simple blocked current u_{scb}.

6. Conclusions

In this paper, we derive analytical expressions that estimate the effect of current on drag force harmonics, which enable an estimate of the blocked current, effective over the structural volume, using only experimental force measurements. Such measurements were obtained by testing a model jacket in combined collinear focused wave groups and current. From analysing these measurements, we conclude that:

(i) Through the use of symmetry and phase inversion to separate Morison drag and inertia forces, we find that measured forces are drag dominated, and that the effects of current are mostly contained in even force frequency harmonics (i.e. the mean and slowly varying second harmonic difference (2−) component, and the second harmonic sum (2+) component that acts at $\sim 2\times$ the peak frequency).

(ii) The (2−) force differs from the other harmonics in that it is asymmetric about the focused wave peak. Inertia contributions are estimated to be small, so we conclude this may be a drag-related fluid memory effect associated with wave-current blockage, but may also be partially caused by error wave contamination.

(iii) By substituting the measured drag forces into the analytical expressions, we estimate the effective blocked currents at the time that the peak wave crest/trough passes through the jacket to be $\sim 40\,\%$ of the undisturbed current speed and roughly half of the estimates using the industry-standard simple current blockage approach. In Appendix D, we estimate that even a lightweight jacket with roughly half the hydrodynamic area (more representative of those supporting offshore wind turbines) blocks $\sim 50\,\%$ of the undisturbed current at the peak wave crest. These estimates were validated by substituting them back into the analytical expressions

https://doi.org/10.1017/jfm.2025.180 Published online by Cambridge University Press

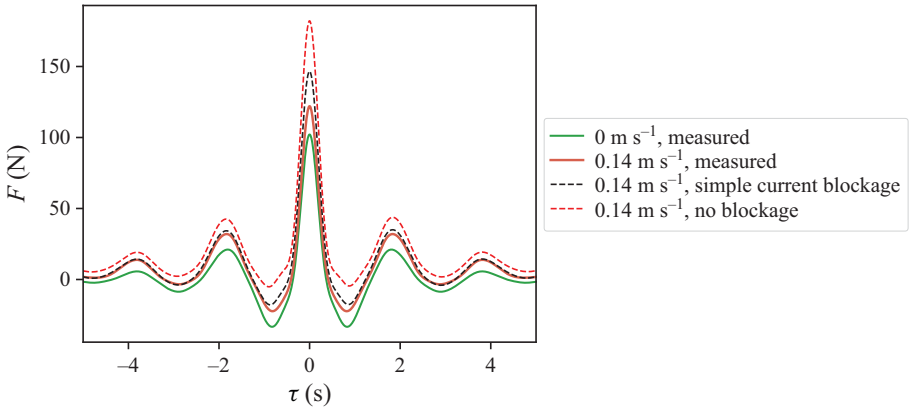

Figure 13. The effect that different assumptions of blocked current have on estimated drag forces. Compared with measured forces with an undisturbed current of $0.14\,\mathrm{m\,s^{-1}}$ (for which we estimate a blocked current u_{cs} at $\tau = 0$ of $u_{cs} = 0.045\ \mathrm{m\,s^{-1}}$), the industry-standard method of simple current blockage (which assumes $u_{cs} = 0.1\ \mathrm{m\,s^{-1}}$) and no blockage (which assumes $u_{cs} = 0.14\ \mathrm{m\,s^{-1}}$) both dramatically over-estimate peak forces. The force time histories for simple current blockage and no blockage were estimated by interpolating measured force time histories, using the estimated time-varying blocked current given by (5.4).

and reconstructing the drag force time histories, showing good agreement with the peak measured drag forces at each current speed.

(iv) The blocked current appears to vary on a similar time scale to the wave envelope, smallest (i.e. most reduced) at the time of peak force, and largest in regions where there are no waves and only current, for which it is given by the simple current blockage model (Taylor 1991). This claim was substantiated by fitting the entire drag force time history with two different analytical models, one that is valid when wave kinematics near the free surface are much larger than current, and one that is valid when wave kinematics are comparatively small. Reconstructed forces agree well with most of the measured force time histories, with poorer agreement localised to intermediate regions where neither analytical model is valid. We explain this current variation with the wave envelope, and why this variation occurs on relatively fast time scales associated with the compact focused wave group, by considering the slowly varying (2−) drag force. This force, which acts as a distributed force dipole on the fluid, creates an upstream flow which reduces the resultant local current speed. As the (2−) forces scale with the wave envelope, so too does the current variation.

The core result of this paper, most relevant for structural engineering, is the reduction in the effective current at the time of peak force. Accounting for this reduced current translates to much lower estimates of peak drag forces, compared with (incorrectly) assuming simple current blockage or no current blockage at all. Figure 13 shows this effect for a $0.14\,\mathrm{m\,s^{-1}}$ undisturbed current, which represents a $1.25\,\mathrm{m\,s^{-1}}$ current at field scale – this can be taken as the associated current for the tested extreme wave with a return period of 1 in ~ 2000 years in the central North Sea. While the magnitude of current and force reduction will change depending on the jacket and wave conditions, the same behaviour may hold in general for all jacket structures in extreme wave and current conditions. We substantiate the possible generality to all jacket structures by testing two jacket configurations, one structurally dense (figure 3) more representative of an oil and gas jacket or an offshore wind substation, and one structurally sparse (figure 15) more representative of those supporting offshore wind turbines. The flow resistances of the

https://doi.org/10.1017/jfm.2025.180 Published online by Cambridge University Press

dense and sparse jackets, characterised by the hydrodynamic drag ratio, $C_d A/A_f$ in (4.1), are 1.4 and 0.85, respectively. According to the international design standard for offshore platforms (API 2000), these flow resistances span a considerable part of the realistic range of jackets installed in the Gulf of Mexico (with hydrodynamic drag coefficients ranging from 0.45 to 1.7).

To conclude, we summarise how this work has contributed to wave-current blockage research, and what gaps still exist. While previous wave-current blockage models rely on computational fluid dynamics simulations which present a significant barrier to adoption in offshore design standards, this work is a step towards the aim of deriving a simpler analytical model. This model may take a form similar to the simple current blockage model (4.1) by Taylor (1991) which only requires knowledge of the structure's geometry and flow resistance, and the incident kinematics. Unlike this idealised model, the analytical expressions derived in this paper require high quality force measurements, which, like computational fluid dynamics simulations, pose a barrier to adoption. Nonetheless, the findings in this paper suggest that it may be possible to derive an adjustment factor that reduces the simple blocked current to account for the extra blockage effect from waves, although more testing is needed to further investigate this claim. This adjustment factor would be easy to incorporate into offshore design standards and, if adopted, would have significant impact on the offshore wind industry – estimated hydrodynamic forces would reduce, so jackets would cost less to make and offshore wind developments would become cheaper.

Acknowledgements. We are thankful to G. Zhao at the Kelvin Hydrodynamics Laboratory for his expertise in collecting high quality data.

Funding. The authors acknowledge support from the ARC ITRH for Transforming energy Infrastructure through Digital Engineering (TIDE, http://TIDE.edu.au) which is led by The University of Western Australia, delivered with The University of Wollongong and several other Australian and International research partners, and funded by the Australian Research Council, INPEX Operations Australia, Shell Australia, Woodside Energy, Fugro Australia Marine, Wood Group Kenny Australia, RPS Group, Bureau Veritas and Lloyd's Register Global Technology (Grant No. IH200100009). A.J.A. acknowledges financial support from a Forrest Research Foundation scholarship and an Australian Government Research Training Program scholarship. H.A.W. was supported by an Australian Research Council (ARC) Early Career Fellowship (DE200101478) and Shell Australia. H.A.W. and J.O. acknowledge the Australian Research Council Linkage Project LP210100397, the Research Impact Grant from the University of Western Australia and the Blue Economy Cooperative Research Centre CRC-20180101, established and supported under the Australian Government's Cooperative Research Centres Program.

Declaration of interests. The authors report no conflict of interest.

Appendix A. Adjusting drag force harmonic expressions for finite jacket depth effects

Jackets are bottom-founded structures; the wave velocity depth integrals in § 2 reflect that the structures extend from the sea bed to above the free surface. In our experiments, however, we submerged the jacket to a depth of 1.33 m in a 1.8 m deep tank, leaving a gap between the base of the jacket and the tank floor. This gap was necessary to prevent the jacket from touching the tank floor whilst being towed. Because the jacket only extended a portion of the water depth, the wave × wave, wave × current and current × current drag force terms in (2.2) should be integrated from the base of the jacket at depth $z = -\alpha h$ to the mean free surface ($z = 0$), where $0 < \alpha < 1$ ($\alpha = 0.74$ for our tests). The resulting drag force expressions are given in table 4. These have the same general structure as the expressions in table 2 but the numerical coefficients for the blocked current

https://doi.org/10.1017/jfm.2025.180 Published online by Cambridge University Press

First harmonic (1)	$\frac{4}{3\pi}\frac{\omega^2 a^2}{k} D_O \left[1+\frac{1}{D_O}\left(4\frac{u_{cs}}{c}+3\frac{\alpha kh}{(ka)^2}\left(\frac{u_{cs}}{c}\right)^2\right)\right]\cos(\phi)$	(A1)
Second harmonic difference (2−)	$\frac{4}{3\pi}\omega^2 a^3\left[1+3\,D_E(ka)^{-2}\frac{u_{cs}}{c}\right]$	(A2)
Second harmonic sum (2+)	$\frac{8}{5\pi}\omega^2 a^3\left[1+5/3\,D_E(ka)^{-2}\frac{u_{cs}}{c}\right]\cos(2\phi)$	(A3)
Third harmonic sum (3+)	$\frac{4}{15\pi}\frac{\omega^2 a^2}{k} D_O \left[1+\frac{1}{D_O}\left(4\frac{u_{cs}}{c}-5\frac{\alpha kh}{(ka)^2}\left(\frac{u_{cs}}{c}\right)^2\right)\right]\cos(3\phi)$	(A4)

Table 4. Drag force frequency harmonic expressions, accounting for the jacket only extending a fraction α of the water depth h. These are of the same form as the expressions in table 2 but the numerical coefficients are adjusted by $D_{\emptyset} = (\alpha kh + (1/2)\sinh(2kh) - (1/2)\sinh(2kh(1-\alpha)))/\sinh^2(kh)$ and $D_E = 1-\sinh(kh(1-\alpha))/\sinh(kh)$.

terms are slightly modified. We used these modified coefficients for the interpretation of wave-current blockage effects from experiments in §§ 5.3 and 5.4.

Appendix B. The accuracy of drag force harmonic expressions for nonlinear wave kinematics

In § 2 we derive approximations for drag force harmonics assuming linear wave kinematics. We argue that, although the assumption of linear kinematics relatively poorly represents the drag forces from waves (as higher-order kinematics are important here), they capture the force amplification from current to sufficient accuracy in the relatively low-order harmonics (≤ 3) as linear wave kinematics dominate the wave × current drag forces. In this appendix, we test the validity of this argument by comparing our drag harmonic expressions with the exact Morison drag solutions using nonlinear wave kinematics for regular waves from Stokes wave theory (Stokes 1847).

Nonlinear wave kinematics were modelled using the full fifth-order Stokes wave theory given by Fenton (1990). At each time t and depth z, the free surface $\eta(t)$ and horizontal wave kinematics $u_w(t, z)$ were calculated for a wave with amplitude $a = 0.21$ m and frequency 0.53 Hz in 1.8 m water depth, hence mirroring the experimental test conditions at the focused wave peak. The modelled Stokes' 5th free surface is shown in figure 14(*a*). Uniform currents u_{cs} of 0.1, 0.05, −0.05 and −0.1 m s^{-1} (similar to the experimental blocked current estimates in table 3) were added to wave kinematics, $u(t, z) = u_w(t, z) + u_{cs}$, and the exact Morison drag force $u(t, z)|u(t, z)|$ was calculated at each depth below the free surface. This was then integrated from the base of the jacket 0.47 m above the tank floor to the fifth-order varying free surface to give the total drag force. Forces were averaged over a 0.15 s moving window to account for the averaging effect over the jacket's width (the model jacket is ∼ 0.45 m wide in the down-wave direction near the mean free surface, which the modelled wave takes ∼ 0.15 s to traverse, hence the total forces are 'smeared' over this time). Finally, the first harmonic (1), second harmonic sum (2+) and difference (2−), and third harmonic sum (3+) drag forces were separated from the total force by digital filtering, as all harmonics are well separated in frequency. The total modelled drag force and its harmonics are shown in figure 14(*b*).

To test the accuracy of our drag harmonic expressions, we essentially replicate the method in § 5.3, treating the Stokes' 5th forces with and without current as experimental

https://doi.org/10.1017/jfm.2025.180 Published online by Cambridge University Press

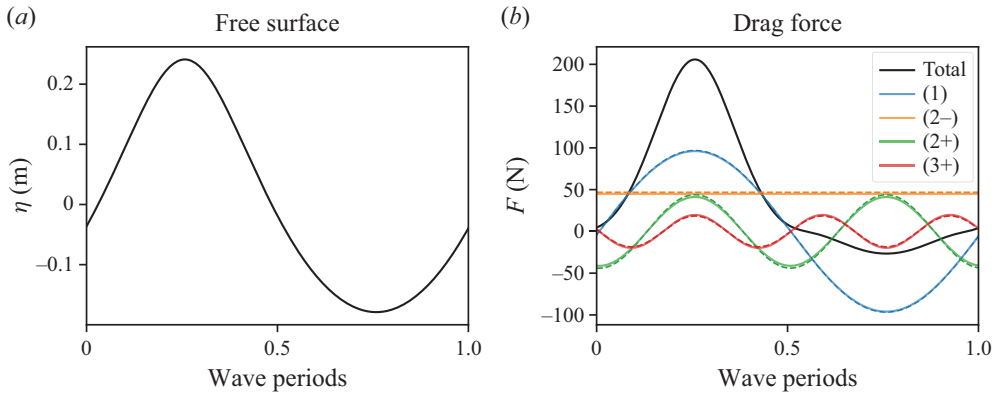

Figure 14. Free surface *(a)* and drag forces *(b)* for a regular wave given by $a = 0.21$ m, $\omega = 3.32$ rad s^{-1} in water depth $h = 1.8$ m, calculated with Stokes fifth-order wave theory by Fenton (1990). In *(b)*, drag forces are calculated with a 0.1 m s^{-1} current. Solid lines represent the exact drag force, while dashed lines represent the approximated drag forces using the pure wave force × [a current multiplier] for each respective harmonic in table 4 (with $u_{cs} = 0.1$ m s^{-1}). Drag forces are scaled by the Morison drag coefficient $1/2\,\rho\, C_d A$, with $\rho = 1000$ kg m^{-3}, $C_d = 0.7$ and $A = 1.12$ m^2, so that the magnitudes of forces are similar to experimental measurements.

Actual (m s^{-1})	**Estimates** (m s^{-1})				% **Difference**
	From (1)	From (2−)	From (2+)	Average	
0.10	0.097	0.093	0.086	0.092	8 %
0.05	0.049	0.046	0.044	0.046	8 %
−0.05	−0.050	−0.045	−0.043	−0.046	9 %
−0.10	−0.094	−0.090	−0.082	−0.089	11 %

Table 5. The accuracy of the drag force harmonic expressions (table 4) in estimating blocked currents. 'Actual' uniform currents were added to Stokes fifth-order wave kinematics, then Morison drag forces were computed and 'estimates' of these currents were made using the drag harmonic expressions. The small % difference between actual and estimated currents demonstrates the accuracy of the method.

force time histories, and using the expressions in table 4 to back calculate the current u_{cs}. These estimates of u_{cs}, given in table 5, are quite accurate, only under-predicting the actual currents by $\sim 10\,\%$. This accuracy can also be observed by the good agreement between the exact and the estimated force harmonics in figure 14(*b*). The under-prediction of currents implies that the experimental u_{cs} estimates in table 3 may be slightly under-predicted, but by a small amount compared with the larger reductions from the undisturbed and simple blocked current estimates. Moreover, if the experimental u_{cs} estimates are indeed slightly under-predicted, the fact that the reconstructed peak drag forces agree well with measured forces in figure 11 indicates that our drag force "recipe" is slightly conservative, which is acceptable in the context of structural design. Overall, this demonstrates that the derived drag force expressions, and consequently the estimates of wave-current blockage effects, are sufficiently accurate for engineering analysis.

Notice that the blocked current estimates in table 5 do not include those using (3+) drag forces. The reason is that we found positive currents have almost no amplification effect (i.e. (3+) wave-only forces are almost identical to (3+) forces with a positive current), hence our method for estimating the blocked current (which relies on this amplification

https://doi.org/10.1017/jfm.2025.180 Published online by Cambridge University Press

factor) has unacceptably large errors. Unlike positive currents, negative currents give some separation of (3+) drag forces so blocked currents can be estimated, which, like the estimates from (1), (2−) and (2+) forces in table 5, under-predict actual current speeds by $\sim 10\,\%$. The null amplification effect on (3+) drag forces from positive currents is partially captured in the analytical (3+) drag force expression (A4) where the u_{cs}^2 term cancels out the u_{cs} term, and is also partially observed in experimental (3+) drag forces (figure 10*g*), but its extent in the Stokes' 5th model is nonetheless a curious result. The (3+) force amplification only slightly changes when we perturb parameters like a and k, suggesting that this effect is not specific to our experimental set-up.

Appendix C. Theoretical drag force harmonics when waves are small compared with current

The analytical drag force harmonics derived in § 2 and Appendix A assume wave kinematics are much larger than the blocked current, hence are only valid for large wave crests/troughs, which for our tests occur at $\tau = 0$. When waves are much smaller, u_{cs} is larger than u_w for most or all of the water column. In our tests, this occurs in the tails of the focused wave groups and particularly for the fastest ± 0.28 m s^{-1} currents. In these regions where $u_w < u_{cs}$, Morison drag (i.e. $(u_w + u_{cs})|u_w + u_{cs}|$ in (1.1)) can be expanded as $\mathrm{sgn}(u_{cs}) \times (u_w^2 + 2u_w u_{cs} + u_{cs}^2)$. Then, similar to the approach in § 2, each component can be integrated across the vertical height of the jacket, $\int_{-\alpha h}^{0} (\cdots)\,\mathrm{d}z$, and across the varying vertical free surface height, $\int_0^{a\cos(\phi)} (\cdots)\,\mathrm{d}z$. The resulting expressions are given in table 6. Considering these expressions apply when wave amplitudes a are small, only two terms are non-negligible, the wave × current depth integral (C3) which acts linearly and the mean current × current term (C5). We make a further simplification by assuming that mean current × current force is equal to the force from current only, $F_{\text{current only}}$, which is approximated by simple current blockage (Taylor 1991). The combined Morison drag force from the two terms is given by (5.5). Note that $F_{\text{current only}}$ depends on the simple blocked current u_{scb} but the wave × current term depends on the (slightly more reduced) blocked current u_{cs}. To explain this choice, we remark that u_{cs} in table 6 expressions is assumed constant with depth, but it actually increases with depth as wave kinematics decay. As waves are small, wave kinematics become very small compared with current only a short distance below the free surface, for which $u_{cs} \approx u_{scb}$. Hence, the current × current force, which is roughly evenly distributed across the jacket's depth, is best modelled using u_{scb}, while the linear wave × current force, which mostly acts near the free surface, is best modelled using u_{cs}.

Appendix D. Wave-current blockage effects for a lightweight jacket

Until now, all experimental results presented in this paper were collected using the model jacket in figure 3. This jacket has a dense array of 24 vertical cylinders that represent conductors on an offshore oil and gas platform or (more crudely) represent J-tubes on an offshore wind electrical substation jacket. This cylinder array contains $\sim 1/2$ of the total hydrodynamic area of the jacket, hence significantly contributes to wave-current blockage effects. Conventional wisdom in offshore engineering is that current blockage effects are not significant on lightweight jackets such as those supporting offshore wind turbines

https://doi.org/10.1017/jfm.2025.180 Published online by Cambridge University Press

Wave × wave term, u_w^2		
Mean depth integral	$\frac{\omega^2 a^2}{4k} D_O \ (1+\cos(2\phi))$	(C1)
Free surface integral	$\frac{\omega^2 a^3}{4} (3\cos(\phi)+\cos(3\phi))$	(C2)
Wave × current term, $2u_w u_{cs}$		
Mean depth integral	$\frac{2\omega a}{k} D_E \, u_{cs} \cos(\phi)$	(C3)
Free surface integral	$\omega a^2 \, u_{cs} \, (1+\cos(2\phi))$	(C4)
Current × current term, u_{cs}^2		
Mean depth integral	$\alpha h \, u_{cs}^2$	(C5)
Free surface integral	$a \, u_{cs}^2 \cos(\phi)$	(C6)

Table 6. Expressions for the mean depth and free surface integrals for the wave × wave, wave × current and current × current Morison drag terms when waves are small compared with current ($u_w < u_{cs}$), accounting for the jacket only extending a fraction α of the water depth h. Note that expansions of the phase components are exact trigonometric expansions rather than being Fourier series representations.

(i.e. jackets without dense structural arrays). In this appendix, we show that this conventional wisdom is false.

We tested the same lightweight jacket used in Archer *et al.* (2024*b*) by removing the 24 vertical conductors – see figure 15(*a*). Using the measured forces in current only and the simple current blockage model (4.1), we estimated the drag coefficient C_d to be 0.87, higher than the denser jacket which has a C_d of 0.7. This increase in C_d may be caused by the lightweight jacket having less shielding (an effect where structural members which trail behind leading members experience reduced forces), and also may be caused by the square horizontal support frame (which has higher C_d compared with cylinders) making up a larger fraction of the total hydrodynamic area. Our method for estimating wave-current blockage effects, however, does not explicitly need C_d, only the measured forces with and without current.

Because of time constraints and different objectives, we only tested undisturbed current speeds u_c of -0.28, -0.14, 0, 0.14 and 0.28 m s^{-1}, and we only ran crest-focused (0° phase) wave groups. For 0 m s^{-1} current, we also ran wave groups that were 60° and 330° phase-shifted. All other aspects of the experimental set-up were the same as in § 3. Like the results in § 4, the experimental measurements were of high quality.

To estimate wave-current blockage effects in the lightweight jacket, we followed a similar method to that discussed in § 5, separating drag and inertia forces and then separating drag forces into its harmonics, to ultimately estimate the blocked current u_{cs} for each current speed. Because the data are more limited, this method had to be slightly adjusted. Namely, harmonic decomposition was only possible for 0 m s^{-1} current for which we ran 0°, 60° and 330° phase-shifted wave groups. Expressions to (partially)

https://doi.org/10.1017/jfm.2025.180 Published online by Cambridge University Press

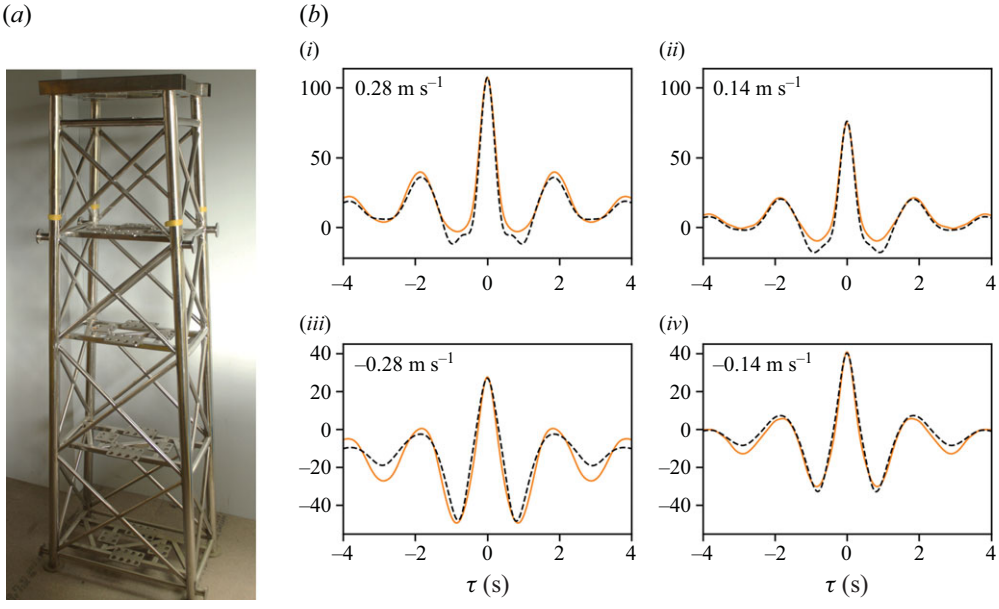

Figure 15. (*a*) Lightweight jacket model with the array of 24 conductors removed. (*b*) Comparison of measured (—) and reconstructed (– –) drag forces. Estimates of u_{cs} given in table 7 were obtained by fitting the peak reconstructed force to the peak measured force.

separate force harmonics are

$$\frac{-(2+\sqrt{3})F_0 - 3F_{0H} + (2-\sqrt{3})F_{60} + \sqrt{3}F_{60H} + (3+\sqrt{3})F_{330}}{2} = \mathbf{(1)} - 2\,\mathbf{(3+)}$$
$$\frac{(4+\sqrt{3})F_0 + 3F_{0H} - (2-\sqrt{3})F_{60} - \sqrt{3}F_{60H} - (3+\sqrt{3})F_{330}}{2} = \mathbf{(2-)} + \mathbf{(2+)} + 3\,\mathbf{(3+)}, \tag{D1}$$

where the subscript H denotes the Hilbert transform, and the bold terms on the right-hand side of the equations denote the frequency harmonics. The top equation gives the linear (1) and 2× the third harmonic sum (3+); the bottom equation gives the second harmonic difference (2−) and sum (2+), and 3× the third harmonic sum. So, the phases do not allow clean separation of harmonics (like regularly spaced 0, 120 and 240 degree phases would), but nonetheless the (2+) and (3+) harmonics can be separated by first filtering (3+) from (1) and then subtracting this from the signal which contains (2−) and (2+). After separating harmonics, the forces from a trough-focused (180°) wave group can be constructed by addition of harmonics, (2−) + (2+) − (1) − (3+) (i.e. relative to crest-focused wave groups, even harmonics are unchanged and odd harmonics are inverted). Then, the drag/inertia separation method (5.2) and subsequently the two-phase combination method (5.1) can be applied, giving the wave-only drag force harmonics. Then, estimates of u_{cs} are obtained by fitting the measured peak drag force for each current speed with the reconstructed force using the expressions in table 4. Finally, the reconstructed drag time histories are shown in figure 15(*b*).

Table 7 lists the u_{cs} estimates for the lightweight jacket, and figure 15(*b*) compares the resulting reconstructed drag force time histories with measurements. u_{cs} estimates for the

https://doi.org/10.1017/jfm.2025.180 Published online by Cambridge University Press

Undisturbed current ($\mathrm{m\,s^{-1}}$)	Estimated u_{cs} ($\mathrm{m\,s^{-1}}$) **Lightweight jacket**	Denser jacket
0.280	**0.14**	0.11
0.140	**0.06**	0.045
−0.140	**−0.09**	−0.071
−0.280	**−0.12**	−0.12

Table 7. Estimated blocked current u_{cs} for the lightweight jacket model in figure 15(*a*). Comparisons are made with the average u_{cs} estimates for the denser jacket given in table 3.

lightweight jacket are $\sim 50\,\%$ of the undisturbed current speed, slightly larger than for the denser jacket ($\sim 40\,\%$). We expected this general trend, as lighter-weight jackets should give less wave-current blockage effects. Still, a reduction of $\sim 50\,\%$ of the undisturbed current speed is significant considering the sparseness of the structure. Because of the lack of data collected for the lightweight jacket compared with the denser jacket, we are less confident in these estimates, but they still indicate that (a) blockage effects for lightweight jackets are still significant and (b) that our methodology for estimating u_{cs} gives sensible results.

References

Allender, J.H. & Petrauskas, C. 1987 Measured and predicted wave plus current loading on a laboratory-scale, space frame structure. In *Offshore Technology Conference, OTC5371*, pp. 143–151.

API 2000 *API 2A-WSD: Recommended Practice for Planning, Designing and Constructing Fixed Offshore Platforms-Working Stress Design*. American Petroleum Institute.

Archer, A.J., Wolgamot, H.A., Draper, S. & Taylor, P.H. 2024*a* A new actuator disc model for oscillatory and steady flow that predicts reductions in jacket drag loads and enhancements in turbine power. *Ocean Engng* **304**, 117881.

Archer, A.J., Wolgamot, H.A., Orszaghova, J., Dai, S. & Taylor, P.H. 2024*b* ADV measurements of blockage flow effects near a model jacket in waves and current. *J. Fluid. Struct.* **125**, 104076.

Cicolin, M.M., Chellini, S., Usherwood, B., Ganapathisubramani, B. & Castro, I.P. 2024 Vortex shedding behind porous flat plates normal to the flow. *J. Fluid Mech.* **985**, A40.

Dalzell, J.F. 1999 A note on finite depth second-order wave–wave interactions. *Appl. Ocean Res.* **21** (3), 105–111.

Fenton, J.D. 1990 Nonlinear wave theories. *The Sea* **9** (1), 3–25.

Fitzgerald, C.J., Taylor, P.H., Eatock Taylor, R., Grice, J. & Zang, J. 2014 Phase manipulation and the harmonic components of ringing forces on a surface-piercing column, *Proc. R. Soc. Lond. A: Math. Phys. Engng Sci.* **470** (2168), 20130847,

Haritos, N. 2007 Introduction to the analysis and design of offshore structures–an overview. *Electron. J. Struct. Engng* **1** (1), 55–65.

ISO 2020 Petroleum and natural gas industries - Fixed steel offshore structures (ISO 19902:2020).

Kristiansen, T. & Faltinsen, O.M. 2017 Higher harmonic wave loads on a vertical cylinder in finite water depth. *J. Fluid Mech.* **833**, 773–805.

Lighthill, J. 1986 Fundamentals concerning wave loading on offshore structures. *J. Fluid Mech.* **173**, 667–681.

Morison, J.R., O'Brien, M.P., Johnson, J.W. & Schaaf, S.A. 1950 The force exerted by surface waves on piles. *J. Petrol. Technol.* **2** (05), 149–154.

Orszaghova, J., Taylor, P.H., Wolgamot, H.A., Madsen, F.J., Pegalajar-Jurado, A.M. & Bredmose, H. 2021 Wave- and drag-driven subharmonic responses of a floating wind turbine. *J. Fluid Mech.* **929**, A32.

Santo, H., Taylor, P.H., Bai, W. & Choo, Y.S. 2015 Current blockage in a numerical wave tank: 3D simulations of regular waves and current through a porous tower. *Comput. Fluids* **115**, 256–269.

Santo, H., Taylor, P.H., Day, A.H., Nixon, E. & Choo, Y.S. 2018*a* Blockage and relative velocity Morison forces on a dynamically-responding jacket in large waves and current. *J. Fluid. Struct.* **81**, 161–178.

https://doi.org/10.1017/jfm.2025.180 Published online by Cambridge University Press

SANTO, H., TAYLOR, P.H., DAY, A.H., NIXON, E. & CHOO, Y.S. 2018*b* Current blockage and extreme forces on a jacket model in focussed wave groups with current. *J. Fluid. Struct.* **78**, 24–35.

SANTO, H., TAYLOR, P.H. & GIBSON, R. 2016 Decadal variability of extreme wave height representing storm severity in the northeast Atlantic and North Sea since the foundation of the Royal Society. *Proc. R. Soc. Lond. A: Math. Phys. Engng Sci.* **472** (2193), 20160376.

SANTO, H., TAYLOR, P.H., WILLIAMSON, C.H.K. & CHOO, Y.S. 2014 Current blockage experiments: force time histories on obstacle arrays in combined steady and oscillatory motion. *J. Fluid Mech.* **739**, 143–178.

SCHÄFFER, H.A. 1996 Second-order wavemaker theory for irregular waves. *Ocean Engng* **23** (1), 47–88.

SEOL, C., KIM, T. & KIM, T. 2024 The effect of permeability on the flow structure of porous square cylinders. *J. Fluid Mech.* **985**, A29.

STOKES, G.G. 1847 On the theory of oscillating waves. *Trans. Camb. Phil. Soc.* **8**, 441–455.

TAYLOR, G.I. 1944 Air resistance of a flat plate of very porous material. *Aero. Res. Counc. R&M* **2236**, 159–162.

TAYLOR, P.H. 1991 Current blockage: reduced forces on offshore space-frame structures. In *Offshore Technology Conference, OTC 6519*.

TAYLOR, P.H., SANTO, H. & CHOO, Y.S. 2013 Current blockage: Reduced Morison forces on space frame structures with high hydrodynamic area, and in regular waves and current. *Ocean Engng* **57**, 11–24.

TAYLOR, P.H., TANG, T., ADCOCK, T.A.A. & ZANG, J. 2024 Transformed-FNV: wave forces on a vertical cylinder — a free-surface formulation. *Coast. Engng* **189**, 104454.

TROMANS, P.S., ANATURK, A.R. & HAGEMEIJER, P. 1991 A new model for the kinematics of large ocean waves - application as a design wave. In *Proceedings of the First 1991 International Offshore and Polar Engineering Conference*.

TROMANS, P.S., HAGEMEIJER, P.M. & WASSINK, H.R. 1992 The statistics of the extreme response of offshore structures. *Ocean Engng* **19** (2), 161–181.

WALKER, D.A.G., TAYLOR, P.H. & EATOCK TAYLOR, R. 2004 The shape of large surface waves on the open sea and the Draupner New Year wave. *Appl. Ocean Res.* **26** (3-4), 73–83.

https://doi.org/10.1017/jfm.2025.180 Published online by Cambridge University Press